Annual Review of Physical Chemistry

Ultrafast Spectroscopy and Dynamics of Photoredox Catalysis

John D. Sakizadeh,[1] Rachel Weiss,[2] Gregory D. Scholes,[1] and Bryan Kudisch[2]

[1]Department of Chemistry, Princeton University, Princeton, New Jersey, USA

[2]Department of Chemistry & Biochemistry, Florida State University, Tallahassee, Florida, USA; email: kudisch@chem.fsu.edu

Annu. Rev. Phys. Chem. 2025. 76:9.1–9.27

The *Annual Review of Physical Chemistry* is online at physchem.annualreviews.org

https://doi.org/10.1146/annurev-physchem-082423-013952

Keywords

photocatalysis, photochemistry, photophysics, time-resolved spectroscopy, transient absorption, electron transfer

Abstract

Photoredox catalysis has emerged as a powerful platform for chemical synthesis, utilizing chromophore excited states as selective energy stores to surmount chemical activation barriers toward making desirable products. Developments in this field have pushed synthetic chemists to design and discover new photocatalysts with novel and impactful photoreactivity but also with uncharacterized excited states and only an approximate mechanistic understanding. This review highlights specific instances in which ultrafast spectroscopies dissected the photophysical and photochemical dynamics of new classes of photoredox catalysts and their photochemical reactions. After briefly introducing the photophysical processes and ultrafast spectroscopic methods central to this topic, the review describes selected recent examples that evoke distinct classes of photoredox catalysts with demonstrated synthetic utility and ultrafast spectroscopic characterization. This review cements the significant role of ultrafast spectroscopy in modern photocatalyzed organic transformations and institutionalizes the developing intersection of synthetic organic chemistry and physical chemistry.

1. INTRODUCTION

Photoredox catalysis is a growing library of photochemical strategies that complement and expand the toolset of modern organic synthesis. Generation of the photocatalyst excited state via photon absorption is central to these photoredox methods, and differentiation between these methods arises from the variety of photocatalysts, substrates, reagents, and cocatalysts present in the reaction mixture to afford an intended product (1–5). Photoredox methodologies for synthesizing a given target are typically mechanistically distinct from the most commonly employed reactions in organic synthesis and leverage photogenerated open-shell intermediates primed for downstream functionalization or integration into other catalytic cycles running in parallel to the photoredox cycle (6–12). As a result, the mechanistic complexities of newly reported photoredox reactions often remain unknown long after reaction discovery, leaving behind questions ranging in scope from the overall per photon efficiency of product formation to the identification of the first productive photochemical reaction step (13, 14). The lack of mechanistic insight can introduce severe bottlenecks in reaction scale-up and optimization that prohibit widespread industrial adoption (15, 16).

Our current mechanistic understanding of photoredox mechanisms stems, in large part, from studies subjecting the reaction mixture to steady-state and time-resolved optical spectroscopies (17, 18). Techniques such as Stern–Volmer photoluminescence quenching (19, 20), photochemical actinometry (21), and nanosecond transient absorption (TA) spectroscopy (22–27) supplied critical missing information about how photoredox reactions proceed upon photon absorption. Photophysical properties of the earliest successful photocatalysts derived from precious metals or fluorescent organic dyes lend themselves to this line of mechanistic inquiry via optical spectroscopy. Their excited states are characterized as photoluminescent, with fluorescence lifetimes longer than 1 ns; for a photochemical reaction, this excited-state lifetime is long enough to engage in a diffusion-controlled photoreaction with a substrate when present at high enough concentrations. For mechanistic studies, photoreaction and subsequent intermediate interconversion and product formation are slow enough to be straightforwardly addressed with nanosecond TA and time-resolved photoluminescence (TRPL) techniques, with many instances demonstrated.

As the field of photoredox catalysis has expanded and novel photocatalysts have been discovered, developed, and implemented for new transformations (23–25, 28–33), it has become clear that photophysical and photochemical processes outpacing the nanosecond or longer timescales of diffusion-controlled reactions play vital roles in reaction mechanisms. Thus, ultrafast spectroscopic methods have emerged as critical tools to reveal the photophysical dynamics of these chromophores and to designate the observed photochemical events as productive or loss pathways. This review focuses on the role of ultrafast spectroscopic techniques in deciphering photoredox mechanisms, bringing particular attention to cases in which photophysical and photochemical processes on the ultrafast timescale profoundly affect the overall photochemical mechanism or the efficiency of the productive photochemical pathway (**Figure 1**). It briefly discusses fundamental photophysical and photochemical processes that precede productive chemical steps or serve as loss pathways, as well as principles underlying the most common and insightful ultrafast spectroscopic approaches utilized in the literature, before reviewing pertinent examples of ultrafast characterization of photoredox catalysts and their dynamics.

2. ULTRAFAST PHOTOINDUCED PROCESSES OF PHOTOREDOX CATALYSTS

The overall efficiency of a photoredox reaction depends on competition between productive pathways, which generate product species or intermediates en route from the substrate to product, and

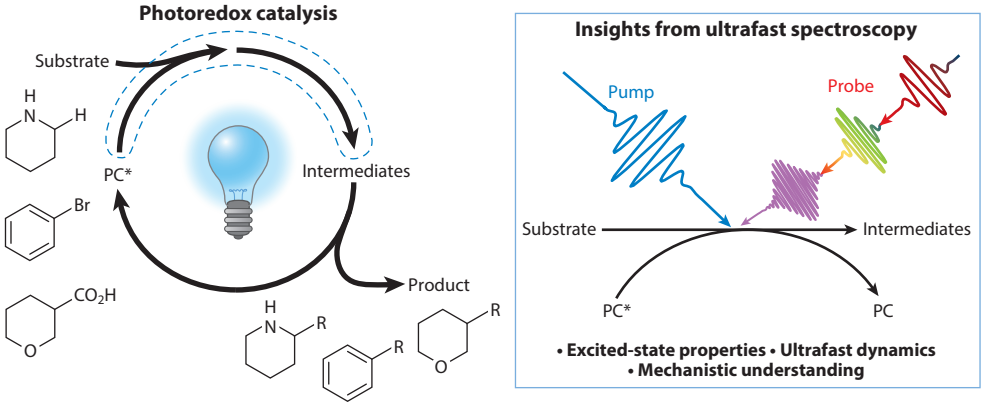

Figure 1

A graphical depiction of the intersection between photoredox catalysis and ultrafast spectroscopy, which is the focus of this review. Abbreviations: PC, photocatalyst ground state; PC*, photocatalyst excited state.

loss pathways, which waste input photonic energy by returning to the ground state or generating an unreactive excited state or side product. The most relevant photophysical pathways occurring on the ultrafast timescale are described in the following subsections. We devote special attention to processes frequently exhibited by metal coordination compounds, which constitute the bulk of the photoredox platforms reviewed herein.

2.1. Intersystem Crossing

Excited states have access to multiple spin configurations depending on the number of electrons occupying distinct molecular orbitals, and the process by which a chromophore changes overall spin multiplicity is termed intersystem crossing (ISC). This process is facilitated by spin–orbit coupling and can approach ultrafast rates depending on the molecular details of the chromophore, such as if heavy atoms are present, if the orbital characters change between initial and final states, and if the states are near degenerate (34). While this process, and the subsequent vibrational cooling, usually steps down the free energy of the photoredox catalyst excited state, the resultant state typically has a much longer excited-state lifetime because of spin-forbidden radiative or nonradiative relaxation pathways to the ground state (phosphorescence or back-ISC, respectively), potentially enabling diffusion-mediated reactivity pathways. Some organic photoredox catalysts undergo ISC to form triplet excited states in the absence of heavy atoms because of charge transfer (CT) configurations that increase the coupling between excited-state spin manifolds (35). Overall, ISC is usually an early, productive photophysical step that a photoredox catalyst takes before substrate photoactivation, with phosphorescence and back-ISC being kinetically sluggish loss pathways.

2.2. Internal Conversion

Excited states can nonradiatively relax to lower energy states of the same spin multiplicity via internal conversion (IC). Strictly speaking, IC (and ISC) is an isoenergetic process, and the energy loss that takes place during these steps is from vibrational relaxation within the vibrational manifold of the newly accessed states. The rate of IC from the lowest-energy excited state to the ground state is typically dictated by Franck–Condon overlap between the excited-state and ground-state vibrational wave functions (36), although the presence of conical intersections can

lead to IC rates much faster than one would predict via the Franck–Condon overlap method (37). IC plays an important role in the excited-state dynamics of transition metal complexes due to low-lying metal-centered [also termed ligand-field (LF)] excited states that can serve as another pathway for rapid depopulation of conventionally photoreactive metal-to-ligand charge transfer (MLCT) or ligand-to-metal charge transfer (LMCT) excited states, depending on the electronic structure of the complex (38, 39). In some cases, IC is accompanied by structural distortions if the excited-state nuclear equilibrium geometries differ greatly between excited states. In the context of photoredox catalysis, IC plays an important role as a loss pathway for both diffusion-limited and preassociated photoredox reactions, although in some literature examples, accessing low-energy, structurally distorted excited states is proposed to be the origin of observed photoreactivity (40).

2.3. Photoinduced Electron Transfer

Excited states and photogenerated intermediates can oxidize or reduce other species in solution via electron transfer (ET), provided that there are sufficient thermodynamic driving force and electronic coupling, with kinetics governed by Marcus theory and its elaborations (41, 42). Photoinduced ET can occur on the subnanosecond timescale if the redox partners are proximal to one another following photoexcitation, by noncovalent association (43), covalent attachment (44, 45), or diffusion if one of the redox partners is present at high concentrations (typically greater than 100 mM) (46). Following photoinduced ET, there is always the possibility of thermodynamically downhill back-ET (also termed charge recombination) to reform the ground electronic states of all species, dissipating input photonic energy as heat to the solvent and furnishing a loss pathway. ET is central to photoredox catalysis, as activation of the substrate or cocatalyst usually involves oxidation or reduction instigated by the photocatalyst excited state, forming high-energy intermediates that can undergo unimolecular or bimolecular reactions to eventually form products. Explicit identification of ultrafast ET processes by spectroscopic methods relies on known spectral information regarding the product of the ET reaction, which can be challenging to independently experimentally verify by nontransient techniques if the intermediates rapidly decompose upon generation, as is often the case for substrates of photoredox reactions (47). In many cases, pulse radiolysis can provide useful reference spectra for radical ion intermediates invoked in photoredox catalytic cycles when steady-state methods fail (48).

2.4. Excitation Energy Transfer

Excited states can nonradiatively transfer their energy to proximal chromophores via excitation energy transfer (EET) processes. Starting from the donor excited state, EET deexcites the donor to the electronic ground state while bringing the acceptor to an electronic excited state. Two mechanisms of EET invoked in photoredox catalysis are the Förster and Dexter mechanisms, the latter of which is typically dominant at close interchromophore distances and with optically dark excited states (49). In analogy to how photosynthetic organisms utilize EET to funnel solar energy from light-harvesting proteins to the photosynthetic reaction center (50), EET strategies to sensitize reactive excited states have been engineered into photoredox platforms (51). This is especially relevant in cases where direct sensitization by photoexcitation is inefficient due to low oscillator strength or a low probability of the optically active state relaxing to the reactive state. Unfortunately, the photophysical details that make EET-based sensitization a useful photochemical strategy can give rise to issues in spectroscopic confirmation of EET as the photochemically relevant mechanism if the final state is challenging to independently prepare in practice. Typically, transition metal complexes engage in energy transfer processes through the Dexter mechanism

due to the low oscillator strength of their high-spin-multiplicity excited states, although specific literature examples featured in this review demonstrate the utility of the typically more rapid Förster mechanism.

2.5. Photoinduced Bond Homolysis/Dissociation

Some molecular excited states are dissociative in nature or feature thermodynamically weak bonds, meaning that upon photoexcitation they can spontaneously and homolytically fragment to form radical intermediates on the ultrafast timescale (52–54). There are many examples of this process when accessing high-energy transitions with UV radiation, but in the visible-wavelength region, relevant to photoredox catalysis, the best model systems are the diatomic halogen-containing molecules and other halogenated organic molecules (55, 56). In the context of photoredox catalysis, the fragmentation process has been spectroscopically documented mostly in transition metal complexes exhibiting LMCT excitation manifolds, where dissociated ligand radicals can serve as an intermediate or a reagent toward an intended transformation. Bond reformation via radical–radical coupling, analogous to back-ET, is a clear loss pathway to this mode of photocatalysis, although spectroscopic investigations into this phenomenon in photoredox contexts are less common than for other ET or EET mechanisms (57).

3. ULTRAFAST SPECTROSCOPIC METHODS

The diverse range of photophysical processes that occur in a photocatalyst following photoexcitation can be addressed with various complementary ultrafast spectroscopic techniques, including some that are not described here but have recently been reviewed elsewhere (58). Central to each technique is the use of a pulsed-laser excitation source, typically with subpicosecond duration, resonant with an electronic absorption feature of the photocatalyst of interest. The use of a laser is followed, at some time delay (ranging from tens of femtoseconds to several nanoseconds), by a range of possible "probe" pulses or spectroscopic readouts that can assess the state of the photoexcited system. The techniques most relevant to photoredox catalysis thus far can be subcategorized into ultrafast optical spectroscopy (59, 60), ultrafast vibrational spectroscopy (61–66), and ultrafast X-ray spectroscopy (67–71), all of which have been extensively reviewed in the broad scope of molecular excited-state dynamics and are schematized in **Figure 2**.

In the context of photoredox catalysis, each technique has its own benefits and drawbacks:

- Ultrafast optical TA spectroscopy is by far the most widespread spectroscopic technique used to study photoredox catalysis due to its relatively straightforward implementation and applicability to a wide variety of photochemical systems, but not all photogenerated species strongly absorb at convenient optical frequencies and optical signatures can be challenging to confidently assign.
- Ultrafast vibrational spectroscopy, such as time-resolved infrared (TRIR) spectroscopy, benefits from its ability to track even minor changes in molecular structure or charge distribution using modifications of vibrational spectra between species, although the low oscillator strengths of most vibrational transitions and increased operational complexity present challenges.
- Ultrafast X-ray spectroscopy takes many forms, including ultrafast absorption, emission, and scattering methods, some of which have found a niche in the photochemical sciences by being able to monitor the ultrafast dynamics of transition metal complexes with individual orbital-level precision; however, these techniques come with high operational complexity and limited accessibility.

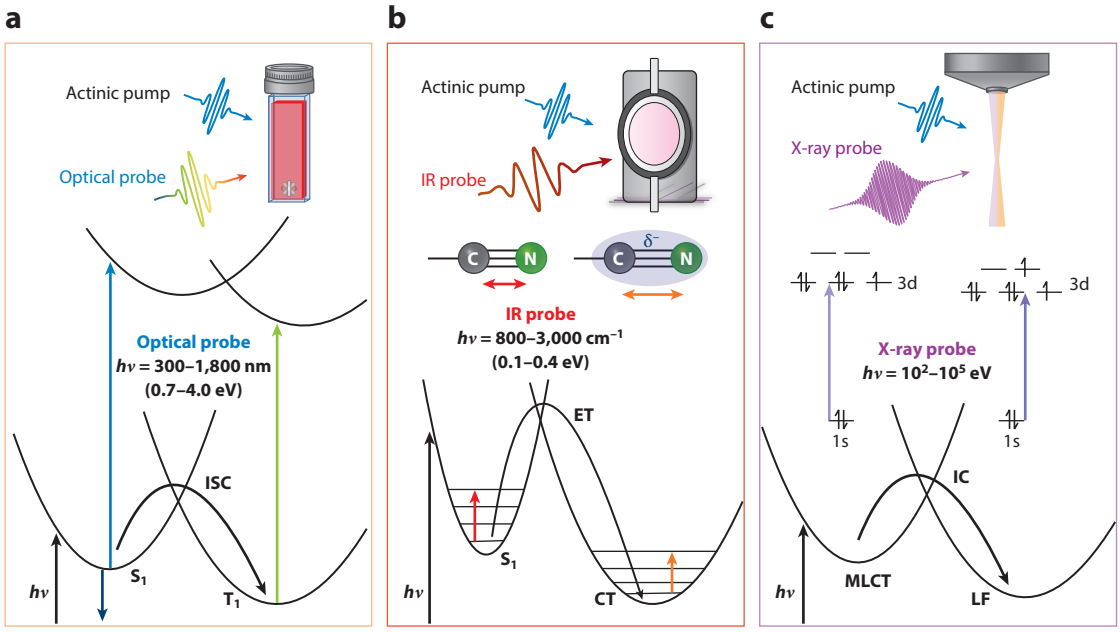

Figure 2

Relevant ultrafast spectroscopic methods used for the study of photoredox catalysis. (*a*) Ultrafast optical spectroscopy. (*b*) Ultrafast vibrational spectroscopy. (*c*) Ultrafast X-ray spectroscopy. Abbreviations: CT, charge transfer; ET, electron transfer; IC, internal conversion; ISC, intersystem crossing; LF, ligand field; MLCT, metal-to-ligand charge transfer.

In each case, transient spectra are typically reported as difference absorption or intensity spectra in the detection frequency range dictated by the technique; thus, each method has independent spectral fingerprints for the various possible photogenerated intermediates. When used in concert with one another, with steady-state characterization techniques, or with computed reference spectra, they are powerful tools for identifying the ultrafast dynamics of a broad range of chromophores, including those relevant to photoredox catalysis.

4. ULTRAFAST DYNAMICS OF PRECIOUS METAL PHOTOREDOX CATALYSTS

Early flash photolysis experiments on precious metal complexes, such as those composed of ruthenium and iridium, revealed the long excited-state lifetime of these complexes, on the order of microseconds, owing to the formation of ^{3}MLCT states, which have spin-forbidden radiative and nonradiative relaxation pathways to the singlet ground state (72). Because of their long excited-state lifetimes and suitable excited-state redox potentials, these complexes found early application as photocatalysts for hydrogen evolution, oxygen reduction, and CO_2 reduction (73, 74). Due to the relatively long timescale for excited-state relaxation in precious metal complexes, early ultrafast characterization studies of these complexes focused on quantifying rates of intrinsically fast processes, such as IC or ISC (75, 76). These early studies observed that quantum yields for ISC within precious metal complexes are near unity and, thus, are not typically a roadblock for increased photoreactivity (77). In contrast, some recent ultrafast characterization studies of precious metal complexes instead focused on direct observation and quantification of subsequent ultrafast dynamics following ISC that are more consequential for overall photoredox reaction efficiency,

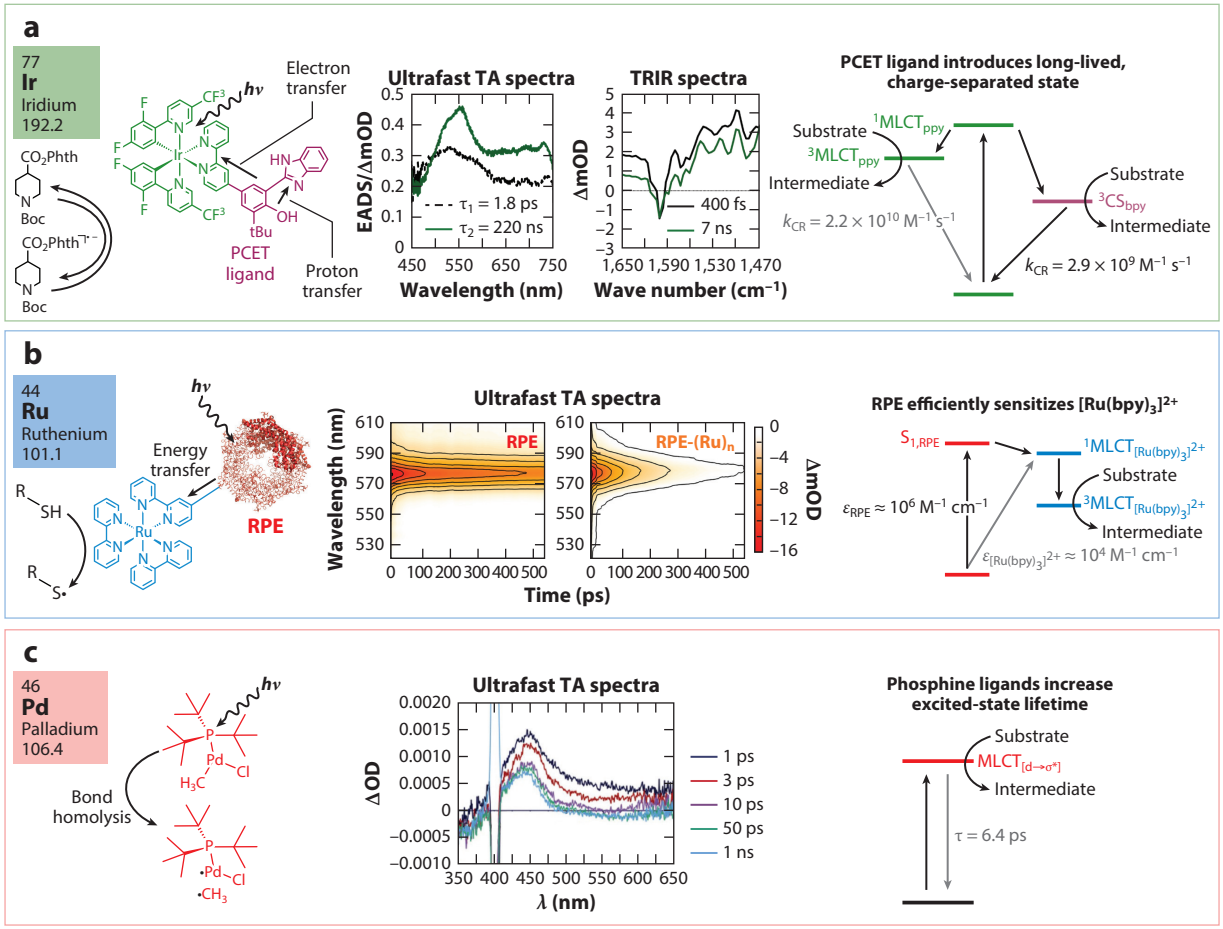

Figure 3

Ultrafast spectroscopic investigations of precious metal photoredox catalysts. (*a*) An iridium photocatalyst connected to a PCET moiety exhibits ultrafast PCET dynamics, generating an intermediate with slower charge recombination than in the absence of the PCET moiety. (*b*) A ruthenium photocatalyst is tethered to a photosynthetic light-harvesting protein for EET-based sensitization of the ruthenium photocatalyst. (*c*) A palladium photocatalyst features a bulky phosphine ligand that slows nonradiative decay processes that compete with palladium–methyl bond homolysis. Abbreviations: CT, charge transfer; EET, excitation energy transfer; ET, electron transfer; LF, ligand field; LMCT, ligand-to-metal charge transfer; MLCT, metal-to-ligand charge transfer; OD, optical density; PCET, proton-coupled electron transfer; RPE, *R*-phycoerythrin. Panel *a* adapted with permission from Reference 79. Panel *b* adapted with permission from Reference 80. Panel *c* adapted from Reference 81 (CC BY 3.0).

such as charge and energy transfer between metal centers and coordinating ligand or covalently bound species (78–80), as well as deactivation processes (81).

An example of an ultrafast process that was designed into a precious metal complex was reported by Sayre et al. (79), who implemented and directly observed ultrafast charge-separated state formation within an Ir(III) photoredox catalyst, [Ir(III)(2-(2,4-difluorophenyl)-5-(trifluoromethyl)pyridil(CF_3)-ppy)$_2$(bpy)]PF_6 (**Figure 3**). Charge-separated state formation was driven by a redox-active benzimidazole–phenol (BIP) substituent on the 2,2-bipyridyl group that coordinates the iridium photocatalyst. The imidazole–phenol pair within BIP is known to facilitate charge separation in metal complex systems through proton-coupled electron transfer (PCET)

and was hypothesized to mitigate charge recombination between the reduced substrate intermediate and the oxidized Ir(III) photocatalyst. Upon excitation of the iridium photoredox catalyst into the MLCT excited state, the BIP moiety reduced the Ir(III) center while simultaneously transferring a proton from the phenol group to the neighboring amide of the benzimidazole group. Ultrafast TA spectra of the Ir(III) complex without the BIP substituent revealed an excited-state absorption (ESA) feature that is associated with the $^3MLCT_{ppy}$ state within 1.5 ps and has an excited-state lifetime of 2.3 μs. Upon addition of the BIP substituent to the Ir(III) complex, Sayre et al. observed a red shift in the ESA feature due to the extended aromatic conjugation from the BIP ligand. Additionally, ultrafast TRIR spectroscopy indicated comparable spectra to infrared spectroelectrochemistry upon electro-oxidation of the iridium complex with the BIP moiety, but not the parent unfunctionalized iridium complex, ultimately allowing the authors to assign the resultant intermediate as a state with oxidized BIP and reduced bipyridine. Doing so resulted in a reduced charge recombination rate between the Ir(III)–BIP complex and the formed intermediate in the photoreduction of methyl viologen (MV^{2+}), relative to the Ir(III) complex without BIP, due to the decreased driving force of BIP oxidation of $MV^{+\bullet}$ in comparison to the oxidized iridium complex. Facilitating ultrafast ET within Ir(III) complexes through the inclusion of redox-active substituents has also found practical application in enhancing the reduction of *N*-hydroxyphthalimide esters (82). In this case, the purposefully introduced ultrafast PCET dynamics clearly influenced downstream productive photochemical events, as confirmed with ultrafast TA and TRIR spectroscopy.

As discussed above, precious metal complexes have excellent photoreactivity and long excited-state lifetimes, but the molar absorptivity of these complexes is often lower than that of organic or biorelevant chromophores. Covalent attachment of the precious metal complex $[Ru(II)(bpy)_3]^{2+}$ to the light-harvesting protein *R*-phycoerythrin (RPE) improves the light absorption efficiency and yields for thiol–ene coupling and cysteinyl desulfurization relative to bare $[Ru(II)(bpy)_3]^{2+}$ (80) (**Figure 3**). Covalent attachment of $[Ru(II)(bpy)_3]^{2+}$ and RPE drove ultrafast EET from the protein to the Ru(II) complex. TRPL kinetics revealed a strong quenching effect in the RPE photoluminescence lifetime from 2.6 ns to 0.4 ns upon attachment of the $[Ru(II)(bpy)_3]^{2+}$ complex, indicating that efficient EET was occurring. Through ultrafast TA spectroscopy, the lifetime of the ground-state bleach (GSB) and stimulated emission signal of RPE decreased from 1.6 ns to 137 ps with incorporation of $[Ru(II)(bpy)_3]^{2+}$ and corroborated the time-resolved fluorescence data. The TA spectra confirmed that EET, and not photoinduced ET, was involved within the RPE-$[Ru(II)(bpy)_3]^{2+}$, since the spectral features following RPE excited-state decay explicitly gave rise to a $[Ru(II)(bpy)_3]^{2+}$ excited-state difference spectrum, not one that corresponds to its oxidation or reduction. The improved light absorption properties of RPE-$[Ru(II)(bpy)_3]^{2+}$ relative to those of bare $[Ru(II)(bpy)_3]^{2+}$ as well as efficient ultrafast EET led to improvements in product yields for photocatalyzed cysteinyl desulfurization and radical thiol–ene reactions when using green or red light-emitting diodes (LEDs), which led to little or no product formation in cases with $[Ru(II)(bpy)_3]^{2+}$ alone.

Waddell et al. (81) recently demonstrated that ultrafast excited-state deactivation processes and methyl radical intermediate formation within Pd(II) organometallic complexes are highly synthetically relevant (**Figure 3**). Their study compared the excited-state dynamics and photoreactivity of a Pd(II) complex coordinated by tri-*tert*-butylphosphine ligands with those of a Pd(II) complex with prototypical α-di-imine ligands. The authors used ultrafast TA spectroscopy to monitor the rates of undesired processes, like IC, that compete with the desired alkyl radical intermediate formation on the ultrafast timescale. Transient spectral features of Pd(II) coordinated by the tri-*tert*-butylphosphine exhibited an excited-state lifetime of 6.4 ps, and the authors observed a long-lived feature associated with complex photodecomposition. The transient spectrum of the

Pd(II) α-di-imine complex had an excited-state lifetime of 3.1 ps that decayed to baseline. The absence of a long-lived feature for this complex indicated insignificant photodegradation. The longer excited-state lifetime of the tri-*tert*-butylphosphine Pd(II) complex strongly suggested slower IC of the excited state to the ground state relative to the α-di-imine Pd(II) complex, and the measured ultrafast excited-state dynamics corresponded to methyl activation quantum yields, which were approximately 0.7 and 0.13 for the tri-*tert*-butylphosphine and α-di-imine Pd(II) complexes, respectively. This study is a particularly pertinent example of ultrafast spectroscopic identification of loss pathways that are directly reflected in overall photochemical reactivity.

5. ULTRAFAST DYNAMICS OF FIRST-ROW TRANSITION METAL PHOTOCATALYSTS

5.1. Iron

Relaxation from MLCT to LF states in first-row transition metal complexes has been believed to limit the photocatalytic activity of these compounds because LF states do not have long lifetimes or are not reactive enough to efficiently perform many photoredox reactions (**Figure 4**). Furthermore, LF excited states are somewhat localized on the metal center, such that the surrounding ligands are thought to create an electronic coupling barrier between the substrate and the redox-active part of the photocatalyst (83). Small LF splitting in first-row analogs to precious metal complexes, like $[Fe(II)(bpy)_3]^{2+}$, leads to relaxation from the initially occupied MLCT states to low-lying LF states on the subpicosecond timescale (84, 85). Ultrafast TA spectroscopic investigations into the photoreactivity of the LF states of $[Fe(II)(bpy)_3]Br_2$ demonstrated that the low reaction QY was due to the short lifetime of the LF state (86). The short-lived nature of the MLCT states of Fe(II) led to the implementation of strategies to increase the reactivity of the LF states of Fe(II) (83, 86). Woodhouse & McCusker (83) showed that decreasing the LF state energy by coordinating Fe(II) with $tren(py)_3$ ligands, which have a small LF splitting, decreased the driving force for excited-state relaxation and resulted in a $[Fe(II)(tren(py)_3)]^{2+}$ complex with a 55 ns excited-state lifetime, allowing it to participate in bimolecular photoinduced ET processes. While this result challenged the paradigm that LF states are functionally inert, the modest driving force for photoinduced ET managed by the LF excited state of $[Fe(II)(tren(py)_3)]^{2+}$ makes many reactions thermodynamically inaccessible.

Alternatively, increasing LF state energies relative to the energies of CT states is a viable strategy to increase CT state lifetimes (87, 88); the Wärnmark group (89, 90) showed that destabilizing the LF states of iron complexes increased the lifetimes of CT states so that they could drive bimolecular photoredox chemistry. In these studies, the authors destabilized the LF states by coordinating Fe(II) and Fe(III) centers with σ-donating *N*-heterocyclic carbene (NHC) ligands that promoted strong LF splitting. The increase in LF splitting decreased the difference between the LF and the MLCT or LMCT state energies and reduced the driving force for relaxation from these CT states to the LF states. While aspects of this research related to excited-state engineering and reaction mechanisms have been reviewed thoroughly elsewhere (91, 92), we focus here on the use of ultrafast characterization to better understand the excited-state dynamics of these complexes in the context of photoredox catalysis.

By tuning the LF state energies, Kjær et al. (93) demonstrated a long-lived CT state of an NHC-coordinated iron complex, $[Fe(III)(phtmeimb)_2]^+$, that could partake in bimolecular photochemistry. Using ultrafast TA spectroscopy and TRPL, they showed that the ^{2}LMCT state of $[Fe(III)(phtmeimb)_2]^+$ has a lifetime of 2 ns (**Figure 4**). The $[Fe(III)(phtmeimb)_2]^+$ complex was also emissive, indicating direct decay from ^{2}LMCT to the ground state. To test the

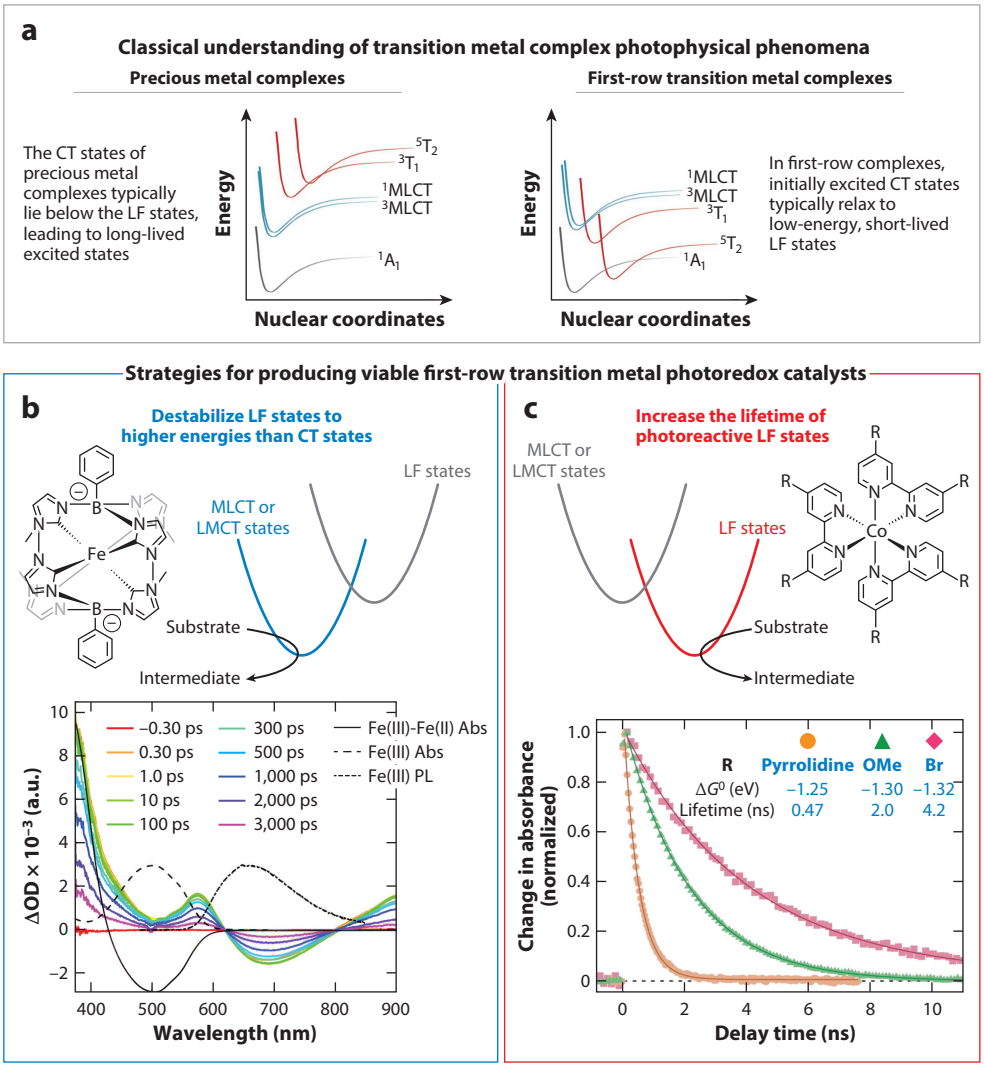

Figure 4

Ultrafast spectroscopy of first-row transition metal photoredox catalysts has identified and characterized reactive states of both CT and LF character. (*a*) Comparison of the photophysical phenomena of precious metal complexes and first-row transition metal complexes shows that the short-lived, low-lying LF states of first-row complexes can lead to challenges in terms of photoredox activity. (*b*) TA spectra of a $[Fe(phtmeimb)^2]^+$ complex reveal the formation of a photoreactive ^{2}LMCT state. (*c*) Single-wavelength decay traces from a series of $[Co(III)(bpy)^3]^{3+}$ with varied substituents demonstrate control over the ^{3}LF state lifetime. Abbreviations: CT, charge transfer; LF, ligand field; LMCT, ligand-to-metal charge transfer; MLCT, metal-to-ligand charge transfer; TA, transient absorption. Panel *a* adapted with permission from Reference 155. Panel *b* adapted with permission from Reference 93. Panel *c* adapted with permission from Reference 103.

photoredox capabilities of $[Fe(III)(phtmeimb)_2]^+$, the authors used the complex to catalyze the reduction of MV^{2+} and oxidation of diphenylamine. To conclusively tie the observed quenching of the $[Fe(III)(phtmeimb)_2]^+$ emission to photoinduced ET reactions, they used TA spectroscopy to observe production of the MV^{2+} and diphenylamine radical intermediates, as evidenced by the emergence of their characteristic spectral signatures.

NHC-coordinated iron complexes, such as $[Fe(III)(btz)_3]^{3+}$ and $[Fe(II)(btz)_3]^{2+}$, also have long-lived excited-state lifetimes (89, 90). Ultrafast TA spectroscopy revealed that the ^{2}LMCT state lifetime of $[Fe(III)(btz)_3]^{3+}$ and the ^{3}MLCT state lifetime of $[Fe(II)(btz)_3]^{2+}$ are 100 ps and 528 ps, respectively (89, 90). The relatively long lifetimes of the photo-oxidative ^{2}LMCT state of $[Fe(III)(btz)_3]^{3+}$ and the photoreductive ^{3}MLCT state of $[Fe(II)(btz)_3]^{2+}$ prompted investigation into coupling these complexes within a single, two-photon catalytic cycle for atom transfer radical addition reactions (94). The first step in the catalytic cycle involved the reduction of photoexcited $[Fe(III)(btz)_3]^{3+}$, forming $[Fe(II)(btz)_3]^{2+}$. Ultrafast TA spectra directly confirmed the initial reduction of photoexcited $[Fe(III)(btz)_3]^{3+}$, showing that reduction of $[Fe(III)(btz)_3]^{3+}$ to $[Fe(II)(btz)_3]^{2+}$ occurs within the ^{2}LMCT state lifetime in the presence of an excess sacrificial electron donor. Subsequent photogeneration of the $[Fe(II)(btz)_3]^{2+}$ ^{3}MLCT state initiated the atom transfer radical addition reaction by reducing an alkyl halide substrate, returning the complex to its $[Fe(III)(btz)_3]^{3+}$ starting state.

Iron photoredox catalysts that do not depend on destabilization of LF states have been studied for their ultrafast photophysical dynamics (95–97). For instance, studies have shown that $Fe(III)Cl_3$ activates C–H bonds, owing to the high reactivity of the in situ–formed chlorine radical upon photoexcitation into its dissociative LMCT state (97). With the intention of designing a more selective C–H activation photocatalyst and better understanding the role of the chlorine radical in C–H bond activation, Gygi et al. (96) studied the photochemistry of Fe(III) chloride–pyridine-di-imine, $[Fe(III)(\text{pyridine-di-imine})Cl_2]^+$. Excitation of $[Fe(III)(\text{pyridine-di-imine})Cl_2]^+$ into the LMCT state generated a chlorine radical capable of promptly abstracting a hydrogen atom from one of the C–H bonds within the second coordination sphere of pyridine-di-imine, indicating stable adduct formation between the chlorine radical and one of the benzene rings on the pyridine-di-imine ligand.

Recognizing that a chlorine radical–pyridine-di-imine adduct was the intermediate responsible for C–H bond activation, the Nocera group (97) employed ultrafast TA spectroscopy to directly monitor adduct formation via its characteristic absorption signal (98). They observed the concurrent emergence of features associated with the chlorine radical–pyridine-di-imine adduct and Fe(II) formation (97). Notably, the decay kinetics of these signals unfolded on distinct timescales; the lifetime of the Fe(II) signal was measured at 1.1 ps, attributed to the reverse reaction involving the chlorine radical and the Fe(II) center, reforming the initial complex. In contrast, the chlorine radical–pyridine-di-imine adduct feature exhibited a longer lifetime of 70 ps, clearly illustrating the stabilizing effect of adduct formation on the chlorine radical and supporting the observation of augmented photoreactivity of this complex.

5.2. Cobalt

Similar to studies surrounding iron complexes, investigations into the ultrafast dynamics of cobalt complexes have focused on controlling LF state energies to increase excited-state lifetimes and photoreactivity. Excited-state engineering strategies that have been successful in the case of Fe(II) and Fe(III) complexes, such as the use of NHC ligands to control LF state energies, can be directly transferred to Co(III) photoredox catalysts (99–101). Because the LF splitting in Co(III) is greater than the splitting of isoelectronic Fe(II) complexes, the LF states of Co(III) complexes are inherently more tunable and expected to be even more redox active, making more reactions accessible from these states (102). However, as discussed above in the context of catalysts like $[Fe(tren(py)_3)]^{2+}$ (83), the difficulty with driving photoredox reactions from LF states is that there is typically a trade-off between the LF state energy and its excited-state lifetime.

The convention that increasing LF state energy comes at the cost of its lifetime was recently challenged by Chan et al. (103), who used ultrafast TA to demonstrate that systematically increasing the LF splitting within a series of $[Co(III)(bpy)_3]^{3+}$ complexes led to increased excited-state lifetimes (**Figure 4**). They explained this result by invoking the Marcus inverted region, which predicts that, upon sufficient destabilization of the LF states, the activation barrier for recombination to reform the ground state increases concomitantly with LF state energy. Leveraging the long lifetime and favorable redox activity of the Co(III) bipyridine chromophores, Chan et al. used the Co(III) complexes to catalyze the bimolecular oxidative coupling of boronic acid and aryl amides, achieving greater product yields in comparison to precious metal Ru(II) and Ir(III) chromophores.

A related study used ultrafast TA spectra to benchmark the strong oxidizing character of the lowest-lying LF state of a Co(III) bipyridine complex, $[Co(III)(4,4'\text{-}Br_2bpy)_3]^{3+}$, which has a lifetime of 4.1 ns (104). GSB recovery kinetics were used to determine the rate of bimolecular quenching of $[Co(4,4'\text{-}Br_2bpy)_3]^{3+}$ by a series of organic substrates with increasing reduction potential. By analyzing the quenching as a function of the oxidation potential of the substrate, the authors of this study estimated the redox potential of the LF state of $[Co(4,4'\text{-}Br_2bpy)_3]^{3+}$ to be 1.25 V versus Fc/Fc^+.

5.3. Nickel

Traditionally, nickel complexes have been employed as cocatalysts alongside exogeneous chromophores to compensate for the short excited-state lifetimes of nickel and drive photoredox chemistry. Working within this constraint, Powers et al. (105) and Jun Hwang et al. (106) used photoredox mediators alongside Ni(II) catalysts to demonstrate a scheme for H_2 evolution. While ultrafast dynamics are likely at play in this system, similar to those discussed above for [Fe(III)(pyridine-di-imine)Cl_2] (96, 97), these studies found that the excited-state lifetime of the nickel complex was too short (<14 ps) to efficiently take part in bimolecular photoredox chemistry when directly photoexcited, and only when coupled with an organic chromophore with a long-lived excited state could the nickel catalyst undergo the appropriate changes in oxidation state to facilitate H_2 evolution.

Despite the original perception that exogenous chromophores are necessary for Ni(II) catalysis, several studies have reported Ni(II) complexes capable of independently driving photoredox reactions, some of which are highlighted in **Figure 5** (40, 107–111). Shields et al. (107) investigated the photophysical mechanisms and photoredox capabilities of the Ni(II) bipyridine aryl halide complex, [Ni(II)(dtbbpy)(*o*-tolyl)Cl], in the context of C–O cross-coupling without an exogenous chromophore. Using ultrafast TA spectroscopy, they found the excited-state lifetime of [Ni(II)(dtbbpy)(*o*-tolyl)Cl] to be 4.1 ns, long enough to partake in diffusion-limited processes. The combination of steady-state spectroscopy and early-time (<10 ps) ultrafast TA spectra supported the assignment of the excited state to a ^{3}MLCT transition, but experimental evidence supporting the idea that the long-lived state was ^{3}MLCT in character was lacking, although the TA spectrum matched a predicted ^{3}MLCT TA spectrum generated using time-dependent density functional theory calculations. In a subsequent study, Ting et al. (40) used ultrafast TA and TRIR spectroscopy to monitor the excited-state dynamics of [Ni(II)(dtbbpy)(*o*-tolyl)Cl]. They collected TRIR spectra from [Ni(II)(dtbbpy)(*o*-tolyl)Cl] with carbonyl-functionalized bipyridine ligand that could report whether the bipyridine ligand was reduced through changes in the C=O infrared stretching frequency. The authors observed that, within 10 ps, there was an ESA signal at reduced frequencies relative to the GSB attributed to reduced bipyridine and, after 10 ps, an ESA feature formed at higher frequencies than the GSB feature, inconsistent with reduced bipyridine.

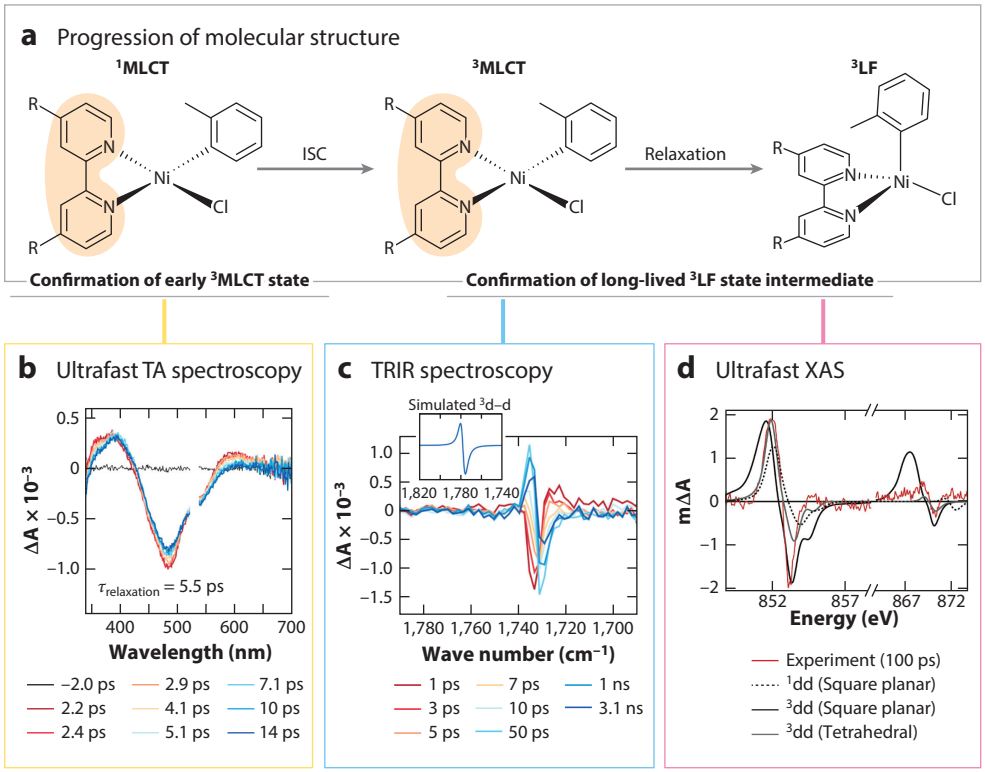

Figure 5

(*a*) Structural evolution of a [Ni(II)(dtbbpy)(*o*-tolyl)Cl] complex after photoexcitation as determined through ultrafast characterization. The Ni(II) complex first undergoes an MLCT transition (with an increase in electron density on the bipyridine ligand; *orange*) and rapid ISC from a ^{1}MLCT to a ^{3}MLCT state. The ^{3}MLCT state then decays to a ^{3}LF state, which persists for several nanoseconds. Ultrafast (*b*) TA spectroscopy, (*c*) TRIR spectroscopy, and (*d*) XAS were used to draw the mechanistic conclusions shown in panel *a*. Abbreviations: ISC, intersystem crossing; LF, ligand field; MLCT, metal-to-ligand charge transfer; TA, transient absorption; TRIR, time-resolved infrared; XAS, X-ray absorption spectroscopy. Panels *b* and *c* adapted with permission from Reference 40. Panel *d* adapted from Reference 112 (CC BY 4.0).

Given that reduced bipyridine is expected for an MLCT transition, this study provided evidence that, while there is an initially formed ^{3}MLCT state, the long-lived state of the complex is a ^{3}LF state (40). This assignment of the long-lived state of [Ni(II)(dtbbpy)(*o*-tolyl)Cl] as a tetrahedral ^{3}LF state has been supported by recent ultrafast X-ray transient absorption (XTA) spectroscopy studies in which the experimental spectrum at 100 ps matched a simulated ^{3}LF transient spectrum (112) (**Figure 5*d***). These reports amount to a unique set of investigations where combinations of ultrafast optical, vibrational, and X-ray spectroscopies fully dissected the excited-state dynamics of a photoactive species leveraged in photoredox catalysis.

However, identifying the state responsible for the photoredox activity of Ni(II) bipyridine aryl halide complexes remains an open debate in the literature. Recent findings indicate that Ni–C bond homolysis, a necessary step in cross-coupling, is not thermodynamically feasible from a ^{3}LF state and that the reaction proceeds through a ^{3}LMCT state (113). The importance of CT states for the cross-coupling activity of Ni(II)–bipyridine aryl halide complexes has prompted investigations into elongating the CT state lifetime of these nickel complexes (108). Bím et al. (108) investigated the photophysical pathways of a Ni(II)–bipyridine aryl halide complex,

[Ni(II)(Phbpy)Cl], with a covalent aryl-bipyridine attachment. This tethering was expected to prevent the complex from relaxing from MLCT to LF states. Ultrafast TA spectra showed that the tethered complex had a longer MLCT lifetime (14 ps) in comparison to the untethered complex (9 ps), with ground-state recovery suggesting that deactivation did not occur via LF states. Reactivity studies indicate that the tethered complex can undergo Ni–C bond homolysis, suggesting that LF states are not the only photocatalytically relevant pathway. However, due to low reaction quantum yields, Ni–C bond homolysis cannot be directly probed via time-resolved spectroscopy.

5.4. Copper

Photoredox implementation of copper-derived photochemistry has mostly leveraged both Cu(I) and Cu(II) oxidation states through divergent photochemical activation pathways, and each oxidation state features unique ultrafast excited-state dynamics that have a substantial impact on their subsequent photochemistry, similar to what has been observed in iron (89, 90) and manganese (114, 115) photocatalysis. Interest in the photoredox properties of Cu(I) complexes stems from its closed-shell $3d^{10}$ ground-state electronic configuration, which prevents deactivation through LF states and extends the lifetimes of the reactive MLCT states (116). However, while the issues related to deactivation through LF states have been bypassed, other unproductive decay pathways exist in Cu(I) complexes; for example, Cu(I) phenanthroline complexes undergo pseudo-Jahn-Teller flattening distortions, which lead to nonradiative decay of the MLCT state (117). To mitigate the flattening distortions that deactivate Cu(I) phenanthroline complexes, the Castellano group (118–120) demonstrated through ultrafast TA spectroscopy how the introduction of steric hindrance through the addition of progressively larger substituents on the phenanthroline ligands of Cu(I) led to distortion resistance, increased excited-state lifetimes, and photoredox activity. In another study, Jayasekara et al. (121) used ultrafast XTA and TA spectroscopy to observe the photophysical mechanism of Cu(I)OTf during a [2+2] photocycloaddition reaction. Ultrafast XTA spectra provided information about both the oxidation state and the coordination environment of the copper center and showed that, upon photoexcitation in the presence of a norbornene substrate, Cu(I)OTf formed a ^{3}MLCT state that preceded the formation of a Cu(II) complex within 100 ps. Complementary ultrafast TA data confirmed that the ^{3}MLCT state formed with a time constant of 4.2 ps.

While Cu(II) complexes have been known to drive photoredox reactions, the presence of low-lying LF excited states and the highly oxidizing nature of their excited states lead to orthogonal photoactivation modalities and shorter excited-state lifetimes of Cu(II) complexes versus Cu(I). In an early investigation of Cu(II) photoreactivity, Kochi (122) argued that, upon photoexcitation, $Cu(II)Cl_2$ undergoes an LMCT transition to form Cu(I)Cl alongside a chlorine radical. The chlorine radical thus generated can drive difficult oxidation reactions, similar to the abovementioned mechanism for LMCT catalysis of $Fe(III)Cl_3$ (96, 97). Given the lack of understanding of Cu(II) LMCT photophysical dynamics in the context of its demonstrated photoreactivity, Mereshchenko et al. (57) used ultrafast TA spectroscopy to monitor the LMCT transition of Cu(II) chloride complexes in acetonitrile, observing that excitation into the LMCT bands of the Cu(II) can lead to formation of Cu(I) and a reactive chlorine radical that kinetically compete with ultrafast relaxation into LF states. These findings were supported in subsequent ultrafast studies by Fayad et al. (123).

In an extension of these fundamental developments, Cu(II) complexes have recently become relevant for decarboxylative coupling reactions driven by LMCT transitions (124, 125). Li et al. (124) reported a versatile, visible-light-driven decarboxylative cross-coupling reaction where they hypothesized that a carboxyl radical forms upon photoexcitation of the Cu(II) complex into a LMCT state. The carboxyl radical was expected to spontaneously eject an equivalent of CO_2,

leaving behind an alkyl radical that can take part in cross-coupling reactions (124). In a subsequent investigation, Chen et al. (125) confirmed the Cu(II) photoredox carboxyl radical formation through ultrafast TA spectroscopy, where they observed the emergence of a carboxyl radical feature within 1 ns after photoexcitation. This developing area of Cu(II) photochemistry via LMCT photoactivation is poised to benefit significantly from future ultrafast spectroscopic studies, with underexplored productive and nonproductive mechanistic pathways kinetically competing on ultrafast timescales.

6. ULTRAFAST DYNAMICS IN SELECT SECOND-ROW, THIRD-ROW, AND CERIUM PHOTOREDOX CATALYSTS

Zhang et al. (126, 127) recently investigated photoactive Zr(IV) complexes that can undergo thermally activated delayed fluorescence (TADF) and can be used as the photosensitizer for photoredox catalysis. To better understand the TADF process within the Zr(IV) complex, [Zr(IV)(^{Mes}PDP)$_2$], they used ultrafast TA spectra to monitor ISC between the initially formed ^{1}LMCT and ^{3}LMCT states (127). Ultrafast TA spectra of [Zr(IV)(^{Mes}PDP)$_2$] revealed the emergence of ESA features within 5 ps, indicating ^{1}LMCT state formation. Over the following 200 ps, the ^{1}LMCT features converted to a broad, long-lived ESA feature that was attributed to ^{3}LMCT state formation. Conversion of the ^{1}LMCT state feature to the ^{3}LMCT feature was accompanied by isosbestic points, indicating that ISC outcompetes direct relaxation to the ground state. Enabled in part by the long lifetime of its ^{3}LMCT state (1.04 ms), [Zr(IV)(^{Mes}PDP)$_2$] was able to drive both reductive and oxidative photochemistry with a series of electron acceptors and donors in addition to isomerization and atom transfer radical addition reactions.

Mo(0) photoredox catalysts are becoming increasingly relevant for their photophysical and catalytic performance, comparable to that of precious metal complexes. Kitzmann et al. (128) used ultrafast TA spectra to characterize excited-state formation within a [Mo(0)(CO)$_3$(tpe)] photoredox catalyst. Ultrafast TA spectra of the Mo(0) complex revealed that a ^{3}MLCT state formed within 0.5 ps after excitation. The observed timescale of the formation of the ^{3}MLCT state was further supported by TRIR spectra of the coordinating ligand Mo(0) complex, which showed the formation of an ESA feature associated with ^{3}MLCT state by 1 ps after excitation. The ^{3}MLCT lifetime of [Mo(0)(Co)$_3$(tpe)] was a few hundred nanoseconds, making it a viable bimolecular photocatalyst, and the complex catalyzed the dehalogenation of chloropyrazine.

$[W_{10}O_{32}]^{4-}$ is an effective photocatalyst for C–H activation, although the excited state responsible for reactivity has not been fully experimentally characterized. Waele et al. (129) aimed to identify the reactive state of a $[W_{10}O_{32}]^{4-}$ complex for hydrogen atom transfer photoreactivity; through ultrafast TA spectroscopy, they simultaneously observed the formation of a GSB feature and an ESA feature, associated with a hot S_1 state, within 0.5 ps. By 1 ps, the ESA feature at 375 nm had narrowed, indicating IC to the S_1 excited state, followed by a decay over the next 100 ps accompanied by a new ESA feature attributable to the previously uncharacterized reactive triplet state with an excited-state lifetime of 50 ns and a 50% quantum yield of formation.

While the above studies focused on excited-state electronic processes, they did not closely monitor the structural changes that take place in the excited state. In a unique example of excited-state structural characterization, Lee et al. (130) used time-resolved X-ray liquidography, which provides structural information on transient intermediates formed after photoexcitation, to characterize the dehalogenation of 1-fluoro-4-iodobenzene using a $[Ce(III)Cl_6]^{3-}$ photoredox catalyst. They attributed the observation of oscillatory features within the difference scattering curves 50 ps after photoexcitation to contraction of the Ce–Cl bonds associated with $[Ce(III)Cl_6]^{3-}$ excited-state formation. In the presence of substrate, excited-state $[Ce(III)Cl_6]^{3-}$ scattering features

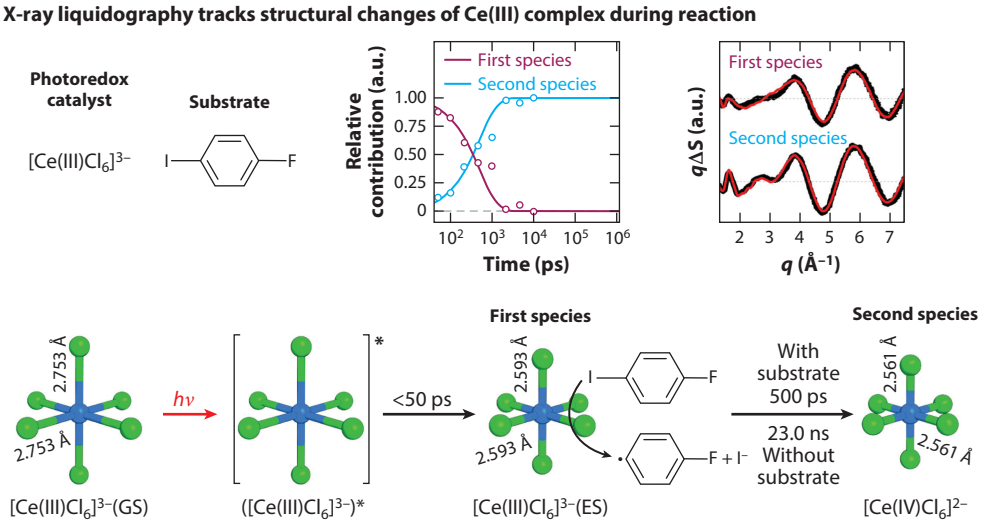

Figure 6

Data and findings from time-resolved X-ray liquidography measurements taken on $[Ce(III)Cl_6]^{3-}$ in the presence and absence of substrate. Figure adapted from Reference 130 (CC BY 4.0).

decayed with a lifetime of 500 ps, giving way to scattering features associated with $[Ce(IV)Cl_6]^{2-}$ (**Figure 6**). The decay of the scattering features of $[Ce(III)Cl_6]^{3-}$ was significantly faster in the presence of substrate than when no substrate was present, where the lifetime was measured to be 9.4 ns; the quenching of the excited-state lifetime of $[Ce(III)Cl_6]^{3-}$ in the presence of substrate was attributed to photoreduction of the substrate. This unique report is one of the first to directly measure the structural changes undergone by a photoredox catalyst following photoactivation of a substrate.

Ce(IV) complexes have been investigated for a series of LMCT-derived photoredox transformations (131), in analogy to those discussed above for Fe(III) and Cu(II) complexes. For example, Hu et al. (132) demonstrated that Ce(IV) alkoxy photoredox catalysts can selectively functionalize light alkanes through photodriven alkoxy radical formation. A subsequent study by An et al. (133) used ultrafast TA spectroscopy to track the alkoxy radical formation process, which occurred on the subpicosecond timescale.

7. ULTRAFAST DYNAMICS IN ORGANIC AND RADICAL PHOTOREDOX CATALYSTS

Practical application of organic photoredox catalysts requires an understanding of how molecular structure dictates excited-state dynamics and, ultimately, overall reactivity. Speckmeier et al. (134) demonstrated that systematic chemical modifications to a donor–acceptor organic photocatalyst can tune its propensity to engage in photoinduced ET. While this study provides a detailed route for relating catalyst structure to reactivity, relatively little research has focused on characterizing the photophysical mechanisms taking place within photoexcited catalysts. As discussed above in relation to transition metal complexes, ultrafast characterization can provide fundamental insights into organic photoredox excited-state properties and reactivity, which are important for bridging catalyst design and performance.

The benefits of investigating the ultrafast excited-state properties of organic photoredox catalysts is evident in studies on phenoxazines and structurally similar molecules that have emerged as

effective atom transfer radical polymerization (ATRP) catalysts (135–137). While earlier studies of organocatalyzed ATRP established empirical relations between the structure of phenoxazine-based molecules and catalytic performance, they neglected experimental investigations into the excited-state dynamics, namely the efficiency of ISC to long-lived triplet states, which are beneficial for reactivity (138). To fill this gap, researchers have used ultrafast TA spectroscopy to understand the influence of structure on the photophysics of a series of phenoxazine catalysts with different aryl substituents (139, 140). This research showed that use of a naphthalene substituent in place of a phenyl substituent can introduce a shallow naphthalene-based CT state that increases the quantum yield of ISC. Other aspects of the organocatalyzed ATRP reaction that have been characterized include photoinitiation and solvent-dependent dynamics using ultrafast TRIR and TA spectra, as well as measurements of the photoinitiation rate with different catalyst substituents (141–143). Counterintuitively, these spectroscopic findings indicate that slower photoinitiation rates lead to greater control over polymer molecular weight and dispersity, establishing new design rules for the organocatalyzed ATRP reaction.

An emerging area in photoredox catalysis is the development of highly reducing or oxidizing chromophores by subjecting a molecular precatalyst to reduction or oxidation, respectively, before photoexcitation (144–147). Radical organic photoredox catalysts have open-shell, doublet excited states. The doublet excited states of these radical organic chromophores have lifetimes on the order of picoseconds or less, which typically prevent them from participating in diffusion-limited photochemistry (148). Because of the short-lived nature of the excited states of radical species, studies investigating their photochemistry have involved preassociation of the radical chromophore with an electron acceptor or donor. Covalent linking of phenothiazine radical cations to electron donors facilitates rapid ET (within 20 ps), as monitored by ultrafast TA spectroscopy (147).

Despite the short-lived excited states of the radical organic chromophores, researchers have reported that they can catalyze bimolecular chemistry (144, 145). Zeman et al. (144) reported a doublet excited state of a perylene di-imide (PDI) radical anion, $^2(PDI^{-\bullet})^*$, that could participate in bimolecular ET reactions. The authors demonstrated that steady-state absorption spectra of neutral PDI and the radical $PDI^{-\bullet}$ had distinct spectral features. Ultrafast TA spectra of $PDI^{-\bullet}$ in the absence of an electron acceptor revealed an ESA signal that decayed with a lifetime of 160 ps alongside the GSB signal. In the presence of an electron acceptor, the ESA feature of $PDI^{-\bullet}$ decayed more rapidly, indicating that the excited state was quenched through the reaction with the electron acceptor (**Figure 7**). The GSB feature did not recover to baseline in the presence of the electron acceptor, indicating that the catalyst was not returning to the $PDI^{-\bullet}$ ground state. The presence of the PDI product was confirmed through the emergence of positive PDI spectral features in the ultrafast TA spectra. PDI TA features were present only when an electron acceptor was used; this finding strongly supports $PDI^{-\bullet}$-driven bimolecular photochemistry. While this study (144) provides clear evidence that radical organic chromophores can catalyze diffusion-limited chemistry, other research has argued that, in some cases, the photoredox activity of doublet excited states may be better explained by in situ conversion of the open-shell radical catalysts to closed-shell analogs, which are known to have comparatively longer excited-state lifetimes (149), or by preassociation of the photoexcited radical with the substrate (150). While many studies have utilized ultrafast spectroscopy to investigate radical photoredox mechanisms, they lack the clear mechanistic evidence established by the Schanze group's (144) investigation of $^2(PDI^{-\bullet})^*$, such as the obvious generation of closed-shell photoproducts of the photosensitizer following interaction with the substrate. Ultrafast spectroscopies will play a vital role in reliably deciphering the mechanisms surrounding these powerful photoredox catalysts.

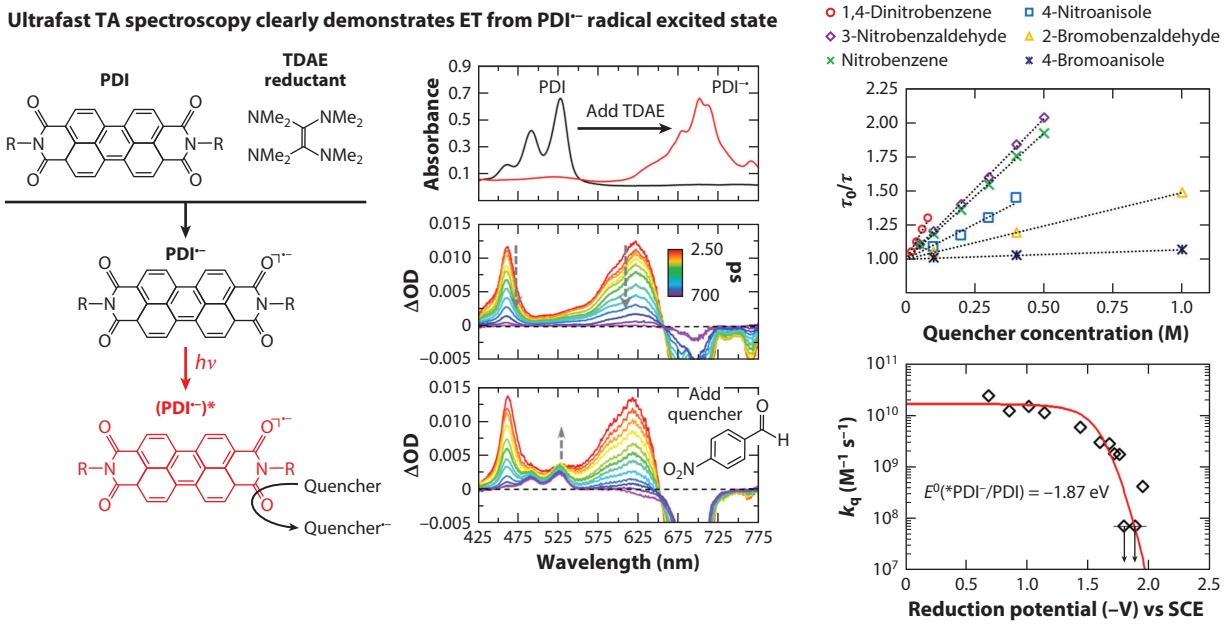

Figure 7

Steady-state and ultrafast TA spectroscopy data of a PDI$^{-\bullet}$ photoredox catalyst with and without a bimolecular quencher alongside the corresponding Rehm–Weller analysis. Abbreviations: ET, electron transfer; OD; optical density; PDI, perylene di-imide; SCE, saturated calomel electrode; TA, transient absorption; TDAE, tetrakis(dimethylamino)ethylene. Figure adapted with permission from Reference 144.

8. CONCLUDING REMARKS AND FUTURE DIRECTIONS

A great deal of progress has been made in characterizing the photophysical and photochemical dynamics of photoredox catalysis using ultrafast techniques. **Supplemental Table 1** highlights many of the photophysical processes featured in this review that have been interrogated on the ultrafast timescale to concisely convey this point.

However, there remain many areas at the intersection of photoredox catalysis and ultrafast spectroscopy that warrant further investigation. Some of them are described below.

8.1. Further Application of Ultrafast X-ray and Vibrational Spectroscopic Techniques

Most of the studies highlighted in this review utilized ultrafast optical spectroscopy to characterize the excited-state dynamics pertinent to photoredox catalysis. As stated above, ultrafast techniques that probe samples using near-UV or visible light typically rely on processes of interest having convenient optical signatures. While ultrafast optical spectroscopy is not ideal for characterizing changes in structure or oxidation state that can take place shortly after excitation, X-ray and vibrational spectroscopy can successfully characterize these processes (151). A recent study demonstrated the utility of these techniques by using ultrafast XTA spectroscopy to show that the long-lived excited state of a Fe(II) complex is of ^{5}LF character (152), although it had originally been identified as a ^{3}MLCT state through other techniques (153). With regard to vibrational spectroscopy, TRIR studies recently helped identify the role of an unexpected transient $N_6^{-\bullet}$ species in what was presumed to be an azidyl radical–mediated C–H activation photoredox reaction (154). To continue to establish the utility of ultrafast X-ray and vibrational spectroscopy

and dive deeper into direct measurement of relevant structural and electronic dynamics in photoredox catalysis, more reports utilizing these techniques need to be added to this growing body of literature.

8.2. Using Coherence as a Tool to Understand Photoredox Excited-State Dynamics

Vibrational coherences observed alongside ultrafast population dynamics can contain information related to vibrational modes important to photochemical processes (155, 156). For example, early experiments in this area showed that vibrational coherences can accompany ET reactions (157, 158) and that suppression of specific vibrational modes that accompany undesired relaxation pathways within a metal complex can lead to an elongated excited-state lifetime (159, 160). However, identification of vibrational modes that may serve as the reaction coordinate for a photoredox reaction is a challenge. Additionally, whether information gained from coherence can be widely applied in the development of our understanding of photoredox catalyst function remains to be determined.

8.3. Ultrafast Characterization of Verifiably Preassociated Systems

Ultrafast techniques are optimal for investigating the excited-state properties of preassociated systems, which typically have fast dynamics relative to bimolecular, diffusion-limited events. Photoenzymes are an example of a preassociated system that has benefited greatly from ultrafast spectroscopic characterization. Ultrafast TA spectroscopy and transient X-ray crystallography have been used to monitor ET from active-site residues (161) or substrates (162) and structural changes within a protein after photoexcitation of a bound cofactor (163), respectively. Success in measuring the excited-state dynamics of these exotic systems motivates further investigation of other underexplored preassociated systems. An example of an underexplored preassociated photoredox platform is electron donor–acceptor complexes that presumably have interesting and mechanistically relevant ultrafast excited-state dynamics but have not yet been deeply spectroscopically characterized (164).

8.4. Discovery and Characterization of Photocatalysts with Unconventional Properties

Insights from recent studies have challenged the notion that long-lived excited states are a necessary characteristic of photoredox catalysts, as evidenced by reports of radical photocatalysts, reactivity derived from metal-centered excited states, and LMCT photoreagents. This new perspective provides an opportunity to revisit metal complexes and organic molecules that had previously been overlooked as potential photocatalysts due to short-lived excited states. Additionally, the development of brighter benchtop LEDs has made it possible to quantitatively drive inefficient reactions that would have not been observed otherwise, such as a recently reported visible-light-driven Birch reduction that required, in some cases, more than 48 h (165). Expanding the library of known photoredox-catalyzed reactions provides additional candidates for mechanistic inquiry through ultrafast spectroscopies, offering new targets for exploration in synthetic chemistry and physical chemistry alike.

DISCLOSURE STATEMENT

The authors are not aware of any affiliations, memberships, funding, or financial holdings that might be perceived as affecting the objectivity of this review.

ACKNOWLEDGMENTS

The writing of this review was supported as part of BioLEC, an Energy Frontier Research Center funded by the US Department of Energy, Office of Science, Basic Energy Sciences under award DE-SC0019370. R.W. and B.K. acknowledge start-up funding from Florida State University.

LITERATURE CITED

1. Shaw MH, Twilton J, MacMillan DWC. 2016. Photoredox catalysis in organic chemistry. *J. Org. Chem.* 81(16):6898–926
2. Prier CK, Rankic DA, MacMillan DWC. 2013. Visible light photoredox catalysis with transition metal complexes: applications in organic synthesis. *Chem. Rev.* 113(7):5322–63
3. Romero NA, Nicewicz DA. 2016. Organic photoredox catalysis. *Chem. Rev.* 116(17):10075–166
4. Narayanam JMR, Stephenson CRJ. 2010. Visible light photoredox catalysis: applications in organic synthesis. *Chem. Soc. Rev.* 40(1):102–13
5. Chan AY, Perry IB, Bissonnette NB, Buksh BF, Edwards GA, et al. 2022. Metallaphotoredox: the merger of photoredox and transition metal catalysis. *Chem. Rev.* 122(2):1485–542
6. Goddard J-P, Ollivier C, Fensterbank L. 2016. Photoredox catalysis for the generation of carbon centered radicals. *Acc. Chem. Res.* 49(9):1924–36
7. Staveness D, Bosque I, Stephenson CRJ. 2016. Free radical chemistry enabled by visible light-induced electron transfer. *Acc. Chem. Res.* 49(10):2295–306
8. Tellis JC, Kelly CB, Primer DN, Jouffroy M, Patel NR, Molander GA. 2016. Single-electron transmetalation via photoredox/nickel dual catalysis: unlocking a new paradigm for sp^3–sp^2 cross-coupling. *Acc. Chem. Res.* 49(7):1429–39
9. Ghosh I, Marzo L, Das A, Shaikh R, König B. 2016. Visible light mediated photoredox catalytic arylation reactions. *Acc. Chem. Res.* 49(8):1566–77
10. Fabry DC, Rueping M. 2016. Merging visible light photoredox catalysis with metal catalyzed C–H activations: on the role of oxygen and superoxide ions as oxidants. *Acc. Chem. Res.* 49(9):1969–79
11. Yoon TP. 2016. Photochemical stereocontrol using tandem photoredox–chiral Lewis acid catalysis. *Acc. Chem. Res.* 49(10):2307–15
12. Hopkinson MN, Tlahuext-Aca A, Glorius F. 2016. Merging visible light photoredox and gold catalysis. *Acc. Chem. Res.* 49(10):2261–72
13. Talbott ED, Burnett NL, Swierk JR. 2023. Mechanistic and kinetic studies of visible light photoredox reactions. *Chem. Phys. Rev.* 4:031312
14. Pitre SP, McTiernan CD, Scaiano JC. 2016. Understanding the kinetics and spectroscopy of photoredox catalysis and transition-metal-free alternatives. *Acc. Chem. Res.* 49(6):1320–30
15. Swierk JR. 2023. The cost of quantum yield. *Org. Process Res. Dev.* 27(7):1411–19
16. Moschetta EG, Cook GC, Edwards LJ, Ischay MA, Lei Z, et al. 2024. Photochemistry in pharmaceutical development: a survey of strategies and approaches to industry-wide implementation. *Org. Process Res. Dev.* 28(4):831–46
17. Arias-Rotondo DM, McCusker JK. 2016. The photophysics of photoredox catalysis: a roadmap for catalyst design. *Chem. Soc. Rev.* 45(21):5803–20
18. Kandoth N, Pérez Hernández J, Palomares E, Lloret-Fillol J. 2021. Mechanisms of photoredox catalysts: the role of optical spectroscopy. *Sustain. Energy Fuels* 5(3):638–65
19. Juneau A, Hope TO, Malenfant J, Mesko M, McNeill J, Frenette M. 2022. Methods to predict potential reagents in iridium-based photoredox catalysis calibrated with stern-volmer quenching rate constants. *ACS Catal.* 12(4):2348–56
20. Soto XL, Swierk JR. 2022. Using lifetime and quenching rate constant to determine optimal quencher concentration. *ACS Omega* 7(29):25532–36
21. Cismesia MA, Yoon TP. 2015. Characterizing chain processes in visible light photoredox catalysis. *Chem. Sci.* 6(10):5426–34
22. Romero NA, Nicewicz DA. 2014. Mechanistic insight into the photoredox catalysis of anti-Markovnikov alkene hydrofunctionalization reactions. *J. Am. Chem. Soc.* 136(49):17024–35

23. Stevenson BG, Spielvogel EH, Loiaconi EA, Wambua VM, Nakhamiyayev RV, Swierk JR. 2021. Mechanistic investigations of an α-aminoarylation photoredox reaction. *J. Am. Chem. Soc.* 143(23):8878–85
24. Ruccolo S, Qin Y, Schnedermann C, Nocera DG. 2018. General strategy for improving the quantum efficiency of photoredox hydroamidation catalysis. *J. Am. Chem. Soc.* 140(44):14926–37
25. Qin Y, Zhu Q, Sun R, Ganley JM, Knowles RR, Nocera DG. 2021. Mechanistic investigation and optimization of photoredox anti-Markovnikov hydroamination. *J. Am. Chem. Soc.* 143(27):10232–42
26. Sun R, Qin Y, Ruccolo S, Schnedermann C, Costentin C, Nocera DG. 2019. Elucidation of a redox-mediated reaction cycle for nickel-catalyzed cross coupling. *J. Am. Chem. Soc.* 141(1):89–93
27. Bhattacherjee A, Sneha M, Lewis-Borrell L, Tau O, Clark IP, Orr-Ewing AJ. 2019. Picosecond to millisecond tracking of a photocatalytic decarboxylation reaction provides direct mechanistic insights. *Nat. Commun.* 10:5152
28. Abderrazak Y, Bhattacharyya A, Reiser O. 2021. Visible-light-induced homolysis of earth-abundant metal–substrate complexes: a complementary activation strategy in photoredox catalysis. *Angew. Chem. Int. Ed.* 60(39):21100–15
29. Juliá F. 2022. Ligand-to-metal charge transfer (LMCT) photochemistry at 3d–metal complexes: an emerging tool for sustainable organic synthesis. *ChemCatChem* 14(19):e202200916
30. Wenger OS. 2018. Photoactive complexes with Earth-abundant metals. *J. Am. Chem. Soc.* 140(42):13522–33
31. Huang H, Steiniger KA, Lambert TH. 2022. Electrophotocatalysis: combining light and electricity to catalyze reactions. *J. Am. Chem. Soc.* 144(28):12567–83
32. Fu H, Hyster TK. 2024. From ground-state to excited-state activation modes: Flavin-dependent "ene" reductases catalyzed non-natural radical reactions. *Acc. Chem. Res.* 57(9):1446–57
33. Glaser F, Kerzig C, Wenger OS. 2020. Multi-photon excitation in photoredox catalysis: concepts, applications, methods. *Angew. Chem. Int. Ed.* 59(26):10266–84
34. Marian CM. 2012. Spin-orbit coupling and intersystem crossing in molecules. *Wiley Interdiscip. Rev. Comput. Mol. Sci.* 2(2):187–203
35. Noda H, Chen X-K, Nakanotani H, Hosokai T, Miyajima M, et al. 2019. Critical role of intermediate electronic states for spin-flip processes in charge-transfer-type organic molecules with multiple donors and acceptors. *Nat. Mater.* 18(10):1084–90
36. Bixon M, Jortner J. 1968. Intramolecular radiationless transitions. *J. Chem. Phys.* 48(2):715–26
37. Schuurman MS, Stolow A. 2018. Dynamics at conical intersections. *Annu. Rev. Phys. Chem.* 69:427–50
38. Wagenknecht PS, Ford PC. 2011. Metal centered ligand field excited states: their roles in the design and performance of transition metal based photochemical molecular devices. *Coord. Chem. Rev.* 255(5/6):591–616
39. Juban EA, Smeigh AL, Monat JE, McCusker JK. 2006. Ultrafast dynamics of ligand-field excited states. *Coord. Chem. Rev.* 250(13/14):1783–91
40. Ting SI, Garakyaraghi S, Taliaferro CM, Shields BJ, Scholes GD, et al. 2020. 3d-d excited states of Ni(II) complexes relevant to photoredox catalysis: spectroscopic identification and mechanistic implications. *J. Am. Chem. Soc.* 142(12):5800–10
41. Gould IR, Farid S. 1996. Dynamics of bimolecular photoinduced electron-transfer reactions. *Acc. Chem. Res.* 29(11):522–28
42. Rather SR, Scholes GD. 2019. From fundamental theories to quantum coherences in electron transfer. *J. Am. Chem. Soc.* 141(2):708–22
43. Ward MD. 1997. Photo-induced electron and energy transfer in non-covalently bonded supramolecular assemblies. *Chem. Soc. Rev.* 26(5):365–75
44. Wasielewski MR. 1992. Photoinduced electron transfer in supramolecular systems for artificial photosynthesis. *Chem. Rev.* 92(3):435–61
45. El-Khouly ME, Ito O, Smith PM, D'Souza F. 2004. Intermolecular and supramolecular photoinduced electron transfer processes of fullerene-porphyrin/phthalocyanine systems. *J. Photochem. Photobiol. C* 5(1):79–104
46. Angulo G, Rosspeintner A. 2020. Bimolecular photo-induced electron transfer enlightened by diffusion. *J. Chem. Phys.* 153:040902

47. Kaim W, Fiedler J. 2009. Spectroelectrochemistry: the best of two worlds. *Chem. Soc. Rev.* 38(12):3373–82
48. Grills DC, Polyansky DE, Fujita E. 2017. Application of pulse radiolysis to mechanistic investigations of catalysis relevant to artificial photosynthesis. *ChemSusChem* 10(22):4359–73
49. Olaya-Castro A, Scholes GD. 2011. Energy transfer from Förster–Dexter theory to quantum coherent light-harvesting. *Int. Rev. Phys. Chem.* 30(1):49–77
50. Mirkovic T, Ostroumov EE, Anna JM, Van Grondelle R, Govindjee Scholes GD. 2017. Light absorption and energy transfer in the antenna complexes of photosynthetic organisms. *Chem. Rev.* 117(2):249–93
51. Strieth-Kalthoff F, James MJ, Teders M, Pitzer L, Glorius F. 2018. Energy transfer catalysis mediated by visible light: principles, applications, directions. *Chem. Soc. Rev.* 47(19):7190–202
52. Harris AL, Brown JK, Harris CB. 1988. The nature of simple photodissociation reactions in liquids on ultrafast time scales. *Annu. Rev. Phys. Chem.* 39:341–66
53. Sato H. 2001. Photodissociation of simple molecules in the gas phase. *Chem. Rev.* 101(9):2687–726
54. Khundkar LR, Zewail AH. 1990. Ultrafast molecular reaction dynamics in real-time: progress over a decade. *Annu. Rev. Phys. Chem.* 41:15–60
55. Han K, He G. 2007. Photochemistry of aryl halides: photodissociation dynamics. *J. Photochem. Photobiol. C* 8(2):55–66
56. Regan PM, Langford SR, Orr-Ewing AJ, Ashfold MNR. 1999. The ultraviolet photodissociation dynamics of hydrogen bromide. *J. Chem. Phys.* 110(1):281–88
57. Mereshchenko AS, Olshin PK, Karimov AM, Skripkin MY, Burkov KA, et al. 2014. Photochemistry of copper(II) chlorocomplexes in acetonitrile: trapping the ligand-to-metal charge transfer excited state relaxation pathways. *Chem. Phys. Lett.* 615:105–10
58. De Kreijger S, Gillard M, Elias B, Troian-Gautier L. 2024. Spectroscopic techniques to unravel mechanistic details in light-induced transformations and photoredox catalysis. *ChemCatChem* 16(1):e202301100
59. Berera R, van Grondelle R, Kennis JTM. 2009. Ultrafast transient absorption spectroscopy: principles and application to photosynthetic systems. *Photosynth. Res.* 101(2/3):105–18
60. Zigmantas D, Polívka T, Persson P, Sundström V. 2022. Ultrafast laser spectroscopy uncovers mechanisms of light energy conversion in photosynthesis and sustainable energy materials. *Chem. Phys. Rev.* 3:041303
61. Nibbering ETJ, Fidder H, Pines E. 2005. Ultrafast chemistry: using time-resolved vibrational spectroscopy for interrogation of structural dynamics. *Annu. Rev. Phys. Chem.* 56:337–67
62. Hamm P, Helbing J, Bredenbeck J. 2008. Two-dimensional infrared spectroscopy of photoswitchable peptides. *Annu. Rev. Phys. Chem.* 59:291–317
63. Fang C, Tang L. 2020. Mapping structural dynamics of proteins with femtosecond stimulated raman spectroscopy. *Annu. Rev. Phys. Chem.* 71:239–65
64. Di Donato M, Groot ML. 2015. Ultrafast infrared spectroscopy in photosynthesis. *Biochim. Biophys. Acta Bioenerg.* 1847(1):2–11
65. van Wilderen LJGW, Bredenbeck J. 2015. From ultrafast structure determination to steering reactions: mixed IR/non-IR multidimensional vibrational spectroscopies. *Angew. Chem. Int. Ed.* 54(40):11624–40
66. Hamaguchi H, Gustafson TL. 1994. Ultrafast time-resolved spontaneous and coherent Raman spectroscopy: the structure and dynamics of photogenerated transient species. *Annu. Rev. Phys. Chem.* 45:593–622
67. Chen LX. 2005. Probing transient molecular structures in photochemical processes using laser-initiated time-resolved X-ray absorption spectroscopy. *Annu. Rev. Phys. Chem.* 56:221–54
68. Miller RJD. 2014. Femtosecond crystallography with ultrabright electrons and X-rays: capturing chemistry in action. *Science* 343(6175):1108–16
69. Chergui M, Collet E. 2017. Photoinduced structural dynamics of molecular systems mapped by time-resolved X-ray methods. *Chem. Rev.* 117(16):11025–65
70. Keefer D, Cavaletto SM, Rouxel JR, Garavelli M, Yong H, Mukamel S. 2023. Ultrafast X-ray probes of elementary molecular events. *Annu. Rev. Phys. Chem.* 74:73–97

71. Bhattacherjee A, Leone SR. 2018. Ultrafast X-ray transient absorption spectroscopy of gas-phase photochemical reactions: a new universal probe of photoinduced molecular dynamics. *Acc. Chem. Res.* 51(12):3203–11
72. Bensasson R, Salet C, Balzani V. 1976. Laser flash spectroscopy of tris(2,2′-bipyridine)ruthenium(II) in solution. *J. Am. Chem. Soc.* 98(12):3722–24
73. Anderson CP, Salmon DJ, Meyer TJ, Young RC. 1977. Photochemical generation of $Ru(bpy)_3^+$ and O_2^-. *J. Am. Chem. Soc.* 99(6):1980–82
74. Ziessel R. 1988. Efficient homogeneous photochemical water gas shift reaction catalysed under extremely mild conditions by novel iridium(III) complexes: $[(\eta^5\text{-}Me_5C_5)Ir(bpy)Cl]^+$, $[(\eta^5\text{-}Me_5C_5)Ir(bpy)H]^+$, and $[(\eta^5\text{-}Me_5C_5)Ir(phen)Cl]^+$ (bpy = 2,2′-bipyridine; phen = 1,10-phenanthroline). *J. Chem. Soc. Chem. Commun.* 1:16–17
75. Damrauer NH, Cerullo G, Yeh A, Boussie TR, Shank CV, McCusker JK. 1997. Femtosecond dynamics of excited-state evolution in $[Ru(bpy)_3]^{2+}$. *Science* 275(5296):54–57
76. Hedley GJ, Ruseckas A, Samuel IDW. 2009. Ultrafast intersystem crossing in a red phosphorescent iridium complex. *J. Phys. Chem. A* 113(1):2–4
77. Crosby GA, Demas JN. 1971. Quantum efficiencies on transition metal complexes. II. Charge-transfer luminescence. *J. Am. Chem. Soc.* 93(12):2841–47
78. Preiß S, Päpcke A, Burkhardt L, Großmann L, Lochbrunner S, et al. 2019. Gold(II) porphyrins in photoinduced electron transfer reactions. *Chem. Eur. J.* 25(23):5940–49
79. Sayre H, Ripberger HH, Odella E, Zieleniewska A, Heredia DA, et al. 2021. PCET-based ligand limits charge recombination with an Ir(III) photoredox catalyst. *J. Am. Chem. Soc.* 143(33):13034–43
80. Cesana PT, Li BX, Shepard SG, Ting SI, Hart SM, et al. 2022. A biohybrid strategy for enabling photoredox catalysis with low-energy light. *Chemistry* 8(1):174–85
81. Waddell PM, Tian L, Scavuzzo AR, Venigalla L, Scholes GD, Carrow BP. 2023. Visible light–induced palladium-carbon bond weakening in catalytically relevant T-shaped complexes. *Chem. Sci.* 14(48):14217–28
82. Guerra WD, Sayre HJ, Ripberger HH, Odella E, Scholes GD, et al. 2022. Ir(III)-naphthoquinone complex as a platform for photocatalytic activity. *J. Photochem. Photobiol.* 9:100098
83. Woodhouse MD, McCusker JK. 2020. Mechanistic origin of photoredox catalysis involving iron(II) polypyridyl chromophores. *J. Am. Chem. Soc.* 142(38):16229–33
84. McCusker JK, Walda KN, Dunn RC, Simon JD, Magde D, Hendrickson DN. 1992. Sub-picosecond $\Delta S = 2$ intersystem crossing in low-spin ferrous complexes. *J. Am. Chem. Soc.* 114(17):6919–20
85. Creutz C, Chou M, Netzel TL, Okumura M, Sutin N. 1980. Lifetimes, spectra, and quenching of the excited states of polypyridine complexes of iron(II), ruthenium(II), and osmium(II). *J. Am. Chem. Soc.* 102(4):1309–19
86. Gualandi A, Marchini M, Mengozzi L, Natali M, Lucarini M, et al. 2015. Organocatalytic enantioselective alkylation of aldehydes with $[Fe(bpy)_3]Br_2$ catalyst and visible light. *ACS Catal.* 5(10):5927–31
87. Steube J, Kruse A, Bokareva OS, Reuter T, Demeshko S, et al. 2023. Janus-type emission from a cyclometalated iron(III) complex. *Nat. Chem.* 15(4):468–74
88. Wellauer J, Ziereisen F, Sinha N, Prescimone A, Velić A, et al. 2024. Iron(III) carbene complexes with tunable excited state energies for photoredox and upconversion. *J. Am. Chem. Soc.* 146(16):11299–318
89. Chábera P, Liu Y, Prakash O, Thyrhaug E, Nahhas AE, et al. 2017. A low-spin Fe(III) complex with 100-ps ligand-to-metal charge transfer photoluminescence. *Nature* 543(7647):695–99
90. Chábera P, Kjaer KS, Prakash O, Honarfar A, Liu Y, et al. 2018. Fe^{II} hexa *N*-heterocyclic carbene complex with a 528 ps metal-to-ligand charge-transfer excited-state lifetime. *J. Phys. Chem. Lett.* 9(3):459–63
91. Glaser F, Aydogan A, Elias B, Troian-Gautier L. 2024. The great strides of iron photosensitizers for contemporary organic photoredox catalysis: on our way to the holy grail? *Coord. Chem. Rev.* 500:215522
92. de Groot LHM, Ilic A, Schwarz J, Wärnmark K. 2023. Iron photoredox catalysis—past, present, and future. *J. Am. Chem. Soc.* 145(17):9369–88
93. Kjær KS, Kaul N, Prakash O, Chábera P, Rosemann NW, et al. 2019. Luminescence and reactivity of a charge-transfer excited iron complex with nanosecond lifetime. *Science* 363(6424):249–53

94. Ilic A, Schwarz J, Johnson C, de Groot LHM, Kaufhold S, et al. 2022. Photoredox catalysis via consecutive ^{2}LMCT- and ^{3}MLCT-excitation of an Fe(III/II)–*N*-heterocyclic carbene complex. *Chem. Sci.* 13(32):9165–75
95. Leis W, Argüello Cordero MA, Lochbrunner S, Schubert H, Berkefeld A. 2022. A photoreactive iron(II) complex luminophore. *J. Am. Chem. Soc.* 144(3):1169–73
96. Gygi D, Gonzalez MI, Hwang SJ, Xia KT, Qin Y, et al. 2021. Capturing the complete reaction profile of a C–H bond activation. *J. Am. Chem. Soc.* 143(16):6060–64
97. Gonzalez MI, Gygi D, Qin Y, Zhu Q, Johnson EJ, et al. 2022. Taming the chlorine radical: enforcing steric control over chlorine-radical-mediated C–H activation. *J. Am. Chem. Soc.* 144(3):1464–72
98. Bühler RE, Ebert M. 1967. Transient charge-transfer complexes with chlorine atoms by pulse radiolysis of carbon tetrachloride solutions. *Nature* 214(5094):1220–21
99. Sinha N, Pfund B, Wegeberg C, Prescimone A, Wenger OS. 2022. Cobalt(III) carbene complex with an electronic excited-state structure similar to cyclometalated iridium(III) compounds. *J. Am. Chem. Soc.* 144(22):9859–73
100. Kaufhold S, Rosemann NW, Chábera P, Lindh L, Bolaño Losada I, et al. 2021. Microsecond photoluminescence and photoreactivity of a metal-centered excited state in a hexacarbene-Co(III) complex. *J. Am. Chem. Soc.* 143(3):1307–12
101. Sinha N, Wenger OS. 2023. Photoactive metal-to-ligand charge transfer excited states in $3d^6$ complexes with Cr^0, Mn^I, Fe^{II}, and Co^{III}. *J. Am. Chem. Soc.* 145(9):4903–20
102. Yarranton JT, McCusker JK. 2022. Ligand-field spectroscopy of Co(III) complexes and the development of a spectrochemical series for low-spin d^6 charge-transfer chromophores. *J. Am. Chem. Soc.* 144(27):12488–500
103. Chan AY, Ghosh A, Yarranton JT, Twilton J, Jin J, et al. 2023. Exploiting the Marcus inverted region for first-row transition metal–based photoredox catalysis. *Science* 382(6667):191–97
104. Alowakennu MM, Ghosh A, McCusker JK. 2023. Direct evidence for excited ligand field state-based oxidative photoredox chemistry of a cobalt(III) polypyridyl photosensitizer. *J. Am. Chem. Soc.* 145(38):20786–91
105. Powers DC, Anderson BL, Nocera DG. 2013. Two-electron HCl to H_2 photocycle promoted by Ni(II) polypyridyl halide complexes. *J. Am. Chem. Soc.* 135(50):18876–83
106. Jun Hwang S, Powers DC, Maher AG, Nocera DG. 2015. Tandem redox mediator/Ni(II) trihalide complex photocycle for hydrogen evolution from HCl. *Chem. Sci.* 6(2):917–22
107. Shields BJ, Kudisch B, Scholes GD, Doyle AG. 2018. Long-lived charge-transfer states of nickel(II) aryl halide complexes facilitate bimolecular photoinduced electron transfer. *J. Am. Chem. Soc.* 140(8):3035–39
108. Bím D, Luedecke KM, Cagan DA, Hadt RG. 2024. Light activation and photophysics of a structurally constrained nickel(II)–bipyridine aryl halide complex. *Inorg. Chem.* 63(9):4120–31
109. Lauenstein R, Mader SL, Derondeau H, Esezobor OZ, Block M, et al. 2021. The central role of the metal ion for photoactivity: Zn- versus Ni-Mabiq. *Chem. Sci.* 12(21):7521–32
110. Cavedon C, Gisbertz S, Reischauer S, Vogl S, Sperlich E, et al. 2022. Intraligand charge transfer enables visible-light-mediated nickel-catalyzed cross-coupling reactions. *Angew. Chem. Int. Ed.* 61(46):e202211433
111. Manafe SY, Le N, Lambert EC, Curiac C, Nugegoda D, et al. 2024. Sensitized and self-sensitized photocatalytic CO_2 reduction to HCO^{2-} and CO under visible light with Ni(II) CNC-pincer catalysts. *ACS Catal.* 14(9):6589–602
112. Wallick RF, Chakrabarti S, Burke JH, Gnewkow R, Chae JB, et al. 2024. Excited-state identification of a nickel-bipyridine photocatalyst by time-resolved X-ray absorption spectroscopy. *J. Phys. Chem. Lett.* 15(18):4976–82
113. Cagan DA, Bím D, Silva B, Kazmierczak NP, McNicholas BJ, Hadt RG. 2022. Elucidating the mechanism of excited-state bond homolysis in nickel-bipyridine photoredox catalysts. *J. Am. Chem. Soc.* 144(14):6516–31
114. East NR, Naumann R, Förster C, Ramanan C, Diezemann G, Heinze K. 2024. Oxidative two-state photoreactivity of a manganese(IV) complex using near-infrared light. *Nat. Chem.* 16(5):827–34
115. Herr P, Kerzig C, Larsen CB, Häussinger D, Wenger OS. 2021. Manganese(I) complexes with metal-to-ligand charge transfer luminescence and photoreactivity. *Nat. Chem.* 13(10):956–62

116. Förster C, Heinze K. 2020. Photophysics and photochemistry with Earth-abundant metals—fundamentals and concepts. *Chem. Soc. Rev.* 49(4):1057–70
117. Shaw GB, Grant CD, Shirota H, Castner EW, Meyer GJ, Chen LX. 2007. Ultrafast structural rearrangements in the MLCT excited state for copper(I) *bis*-phenanthrolines in solution. *J. Am. Chem. Soc.* 129(7):2147–60
118. Garakyaraghi S, Danilov EO, McCusker CE, Castellano FN. 2015. Transient absorption dynamics of sterically congested Cu(I) MLCT excited states. *J. Phys. Chem. A* 119(13):3181–93
119. McCusker CE, Castellano FN. 2013. Design of a long-lifetime, Earth-abundant, aqueous compatible Cu(I) photosensitizer using cooperative steric effects. *Inorg. Chem.* 52(14):8114–20
120. Khnayzer RS, McCusker CE, Olaiya BS, Castellano FN. 2013. Robust cuprous phenanthroline sensitizer for solar hydrogen photocatalysis. *J. Am. Chem. Soc.* 135(38):14068–70
121. Jayasekara GK, Antolini C, Smith MA, Jacoby DJ, Escolastico J, et al. 2021. Mechanisms of the Cu(I)-catalyzed intermolecular photocycloaddition reaction revealed by optical and X-ray transient absorption spectroscopies. *J. Am. Chem. Soc.* 143(46):19356–64
122. Kochi JK. 1962. Photolyses of metal compounds: cupric chloride in organic media. *J. Am. Chem. Soc.* 84(11):2121–27
123. Fayad R, Engl S, Danilov EO, Hauke CE, Reiser O, Castellano FN. 2020. Direct evidence of visible light–induced homolysis in chlorobis(2,9-dimethyl-1,10-phenanthroline)copper(II). *J. Phys. Chem. Lett.* 11(13):5345–49
124. Li QY, Gockel SN, Lutovsky GA, DeGlopper KS, Baldwin NJ, et al. 2022. Decarboxylative cross-nucleophile coupling via ligand-to-metal charge transfer photoexcitation of Cu(II) carboxylates. *Nat. Chem.* 14(1):94–99
125. Chen TQ, Pedersen PS, Dow NW, Fayad R, Hauke CE, et al. 2022. A unified approach to decarboxylative halogenation of (hetero)aryl carboxylic acids. *J. Am. Chem. Soc.* 144(18):8296–305
126. Zhang Y, Petersen JL, Milsmann C. 2016. A luminescent zirconium(IV) complex as a molecular photosensitizer for visible light photoredox catalysis. *J. Am. Chem. Soc.* 138(40):13115–18
127. Zhang Y, Lee TS, Favale JM, Leary DC, Petersen JL, et al. 2020. Delayed fluorescence from a zirconium(IV) photosensitizer with ligand-to-metal charge-transfer excited states. *Nat. Chem.* 12(4):345–52
128. Kitzmann WR, Bertrams M-S, Boden P, Fischer AC, Klauer R, et al. 2023. Stable molybdenum(0) carbonyl complex for upconversion and photoredox catalysis. *J. Am. Chem. Soc.* 145(30):16597–609
129. Waele VD, Poizat O, Fagnoni M, Bagno A, Ravelli D. 2016. Unraveling the key features of the reactive state of decatungstate anion in hydrogen atom transfer (HAT) photocatalysis. *ACS Catal.* 6(10):7174–82
130. Lee Y, Ki H, Im D, Eom S, Gu J, et al. 2023. Cerium photocatalyst in action: structural dynamics in the presence of substrate visualized via time-resolved X-ray liquidography. *J. Am. Chem. Soc.* 145(43):23715–26
131. Zhao R, Shi L. 2018. A renaissance of ligand-to-metal charge transfer by cerium photocatalysis. *Org. Chem. Front.* 5(20):3018–21
132. Hu A, Guo J, Pan H, Zuo Z. 2018. Selective functionalization of methane, ethane, and higher alkanes by cerium photocatalysis. *Science* 361(6403):668–72
133. An Q, Wang Z, Chen Y, Wang X, Zhang K, et al. 2020. Cerium-catalyzed C–H functionalizations of alkanes utilizing alcohols as hydrogen atom transfer agents. *J. Am. Chem. Soc.* 142(13):6216–26
134. Speckmeier E, Fischer TG, Zeitler K. 2018. A toolbox approach to construct broadly applicable metal-free catalysts for photoredox chemistry: deliberate tuning of redox potentials and importance of halogens in donor-acceptor cyanoarenes. *J. Am. Chem. Soc.* 140(45):15353–65
135. Pearson RM, Lim C-H, McCarthy BG, Musgrave CB, Miyake GM. 2016. Organocatalyzed atom transfer radical polymerization using *N*-aryl phenoxazines as photoredox catalysts. *J. Am. Chem. Soc.* 138(35):11399–407
136. Theriot JC, Lim C-H, Yang H, Ryan MD, Musgrave CB, Miyake GM. 2016. Organocatalyzed atom transfer radical polymerization driven by visible light. *Science* 352(6289):1082–86
137. Corbin DA, Miyake GM. 2022. Photoinduced organocatalyzed atom transfer radical polymerization (O-ATRP): precision polymer synthesis using organic photoredox catalysis. *Chem. Rev.* 122(2):1830–74

138. McCarthy BG, Pearson RM, Lim C-H, Sartor SM, Damrauer NH, Miyake GM. 2018. Structure-property relationships for tailoring phenoxazines as reducing photoredox catalysts. *J. Am. Chem. Soc.* 140(15):5088–101
139. Sartor SM, McCarthy BG, Pearson RM, Miyake GM, Damrauer NH. 2018. Exploiting charge-transfer states for maximizing intersystem crossing yields in organic photoredox catalysts. *J. Am. Chem. Soc.* 140(14):4778–81
140. Sartor SM, Lattke YM, McCarthy BG, Miyake GM, Damrauer NH. 2019. Effects of naphthyl connectivity on the photophysics of compact organic charge-transfer photoredox catalysts. *J. Phys. Chem. A* 123(22):4727–36
141. Orr-Ewing AJ. 2019. Perspective: How can ultrafast laser spectroscopy inform the design of new organic photoredox catalysts for chemical and materials synthesis? *Struct. Dyn.* 6:010901
142. Koyama D, Dale HJA, Orr-Ewing AJ. 2018. Ultrafast observation of a photoredox reaction mechanism: photoinitiation in organocatalyzed atom-transfer radical polymerization. *J. Am. Chem. Soc.* 140(4):1285–93
143. Bhattacherjee A, Sneha M, Lewis-Borrell L, Amoruso G, Oliver TAA, et al. 2021. Singlet and triplet contributions to the excited-state activities of dihydrophenazine, phenoxazine, and phenothiazine organocatalysts used in atom transfer radical polymerization. *J. Am. Chem. Soc.* 143(9):3613–27
144. Zeman CJ, Kim S, Zhang F, Schanze KS. 2020. Direct observation of the reduction of aryl halides by a photoexcited perylene diimide radical anion. *J. Am. Chem. Soc.* 142(5):2204–7
145. MacKenzie IA, Wang L, Onuska NPR, Williams OF, Begam K, et al. 2020. Discovery and characterization of an acridine radical photoreductant. *Nature* 580(7801):76–80
146. Baek Y, Reinhold A, Tian L, Jeffrey PD, Scholes GD, Knowles RR. 2023. Singly reduced iridium chromophores: synthesis, characterization, and photochemistry. *J. Am. Chem. Soc.* 145(23):12499–508
147. Christensen JA, Phelan BT, Chaudhuri S, Acharya A, Batista VS, Wasielewski MR. 2018. Phenothiazine radical cation excited states as super-oxidants for energy-demanding reactions. *J. Am. Chem. Soc.* 140(15):5290–99
148. Gumy J-C, Vauthey E. 1997. Investigation of the excited-state dynamics of radical ions in the condensed phase using the picosecond transient grating technique. *J. Phys. Chem. A* 101(46):8575–80
149. Rieth AJ, Gonzalez MI, Kudisch B, Nava M, Nocera DG. 2021. How radical are "radical" photocatalysts? A closed-shell Meisenheimer complex is identified as a super-reducing photoreagent. *J. Am. Chem. Soc.* 143(35):14352–59
150. Pfund B, Gejsnæs-Schaad D, Lazarevski B, Wenger OS. 2024. Picosecond reactions of excited radical ion super-reductants. *Nat. Commun.* 15:4738
151. Gaffney KJ. 2021. Capturing photochemical and photophysical transformations in iron complexes with ultrafast X-ray spectroscopy and scattering. *Chem. Sci.* 12(23):8010–25
152. Reinhard ME, Sidhu BK, Lozada IB, Powers-Riggs N, Ortiz RJ, et al. 2024. Time-resolved X-ray emission spectroscopy and synthetic high-spin model complexes resolve ambiguities in excited-state assignments of transition-metal chromophores: a case study of Fe-amido complexes. *J. Am. Chem. Soc.* 146(26):17908–16
153. Braun JD, Lozada IB, Kolodziej C, Burda C, Newman KME, et al. 2019. Iron(II) coordination complexes with panchromatic absorption and nanosecond charge-transfer excited state lifetimes. *Nat. Chem.* 11(12):1144–50
154. Sneha M, Thornton GL, Lewis-Borrell L, Ryder ASH, Espley SG, et al. 2023. Photoredox-HAT catalysis for primary amine α-C-H alkylation: mechanistic insight with transient absorption spectroscopy. *ACS Catal.* 13(12):8004–13
155. Scholes GD, Fleming GR, Chen LX, Aspuru-Guzik A, Buchleitner A, et al. 2017. Using coherence to enhance function in chemical and biophysical systems. *Nature* 543(7647):647–56
156. McCusker JK. 2019. Electronic structure in the transition metal block and its implications for light harvesting. *Science* 363(6426):484–88
157. Rather SR, Fu B, Kudisch B, Scholes GD. 2021. Interplay of vibrational wavepackets during an ultrafast electron transfer reaction. *Nat. Chem.* 13(1):70–76
158. Yoneda Y, Kudisch B, Rather SR, Maiuri M, Nagasawa Y, et al. 2021. Vibrational dephasing along the reaction coordinate of an electron transfer reaction. *J. Am. Chem. Soc.* 143(36):14511–22

159. Paulus BC, Adelman SL, Jamula LL, McCusker JK. 2020. Leveraging excited-state coherence for synthetic control of ultrafast dynamics. *Nature* 582(7811):214–18
160. Schrauben JN, Dillman KL, Beck WF, McCusker JK. 2010. Vibrational coherence in the excited state dynamics of $Cr(acac)_3$: probing the reaction coordinate for ultrafast intersystem crossing. *Chem. Sci.* 1(3):405–10
161. Li X, Page CG, Zanetti-Polzi L, Kalra AP, Oblinsky DG, et al. 2023. Mechanism and dynamics of photodecarboxylation catalyzed by lactate monooxygenase. *J. Am. Chem. Soc.* 145(24):13232–40
162. Wu R, Li X, Wang L, Zhong D. 2022. Ultrafast dynamics and catalytic mechanism of fatty acid photodecarboxylase. *Angew. Chem. Int. Ed.* 61(50):e202209180
163. Sorigué D, Hadjidemetriou K, Blangy S, Gotthard G, Bonvalet A, et al. 2021. Mechanism and dynamics of fatty acid photodecarboxylase. *Science* 372(6538):eabd5687
164. Crisenza GEM, Mazzarella D, Melchiorre P. 2020. Synthetic methods driven by the photoactivity of electron donor-acceptor complexes. *J. Am. Chem. Soc.* 142(12):5461–76
165. Cole JP, Chen D-F, Kudisch M, Pearson RM, Lim C-H, Miyake GM. 2020. Organocatalyzed birch reduction driven by visible light. *J. Am. Chem. Soc.* 142(31):13573–81